KINETIC MODELLING OF FAST CATALYTIC PYROLYSIS OF BIOMASS

A THESIS

Submitted by

ABHIJEET PRABHAKARRAO SELUKAR

(ROLL NO. CA21M001)

in partial fulfilment of requirements for

MASTER OF TECHNOLOGY

DEPARTMENT OF CHEMICAL ENGINEERING

INDIAN ISTITUTE OF TECHNOLOGY MADRAS

CHENNAI-600 036

MAY 2023

Table of Contents

List of Figures

List of Tables

Abstract

Keywords: Biomass, Pyrolysis, Catalytic, kinetic studies, Master plot

This study involves kinetic analysis of Fast pyrolysis and fast catalytic pyrolysis reactions. Different methods for kinetic analysis under various conditions were discussed. The pyrolysis behaviour of cellulose, straw, and sawdust biomass was studied using the model free iso-conversional method under three conditions:

1) in the absence of Catalyst 2) with Ni-CaO-Si_2O_4 Catalyst and 3) with Ni-Ca_2SiO_4 Catalyst to Calculating the kinetic parameters five model free isoconversional methods are used And five model free isoconversional methods are 1) Distributed Activation Energy (DAEM) Model 2)Kissinger-Akhira-Sunose (KAS), 3) Starink, and 4) Flynn-Wall-Ozawa (FWO) and 5)Friedman Method. In this work, we employed these five techniques to investigate the influence of Activation Energy, Pre-exponential Factor on various conditions. And did a comparative study of kinetic parameters. And in case of Straw and Cellulose showed significant effect in case of Ni-$CaOSi_2O_4$ conditions while in case of Sawdust at the final conversion stages it showed more catalytic effect by decreasing the activation energy in case of Ni-Ca_2SiO_4 condition, and to understand the reaction mechanism used the master plot. And significant impact of catalysts showed on the reaction mechanisms. The use of $NiCaOSi_2O_4$ catalyst altered the reaction pathway, with involvement of nucleation, diffusion control, and multiple reaction mechanisms.

1. Introduction

Rising energy consumption, particularly in the transportation sector, and rising CO_2 emissions need the use of renewable energy sources. Despite the numerous novel energy carriers, liquid hydrocarbon appears to be the most appealing and viable kind of transportation fuel when energy density, stability, and existing infrastructure are considered. Biomass is a plentiful, renewable source of energy; nevertheless, harnessing biomass in a cost-effective manner remains a significant difficulty. Lignocellulose is made up of three main biopolymers: cellulose, hemicellulose, and lignin. Fast pyrolysis of biomass has been identified as an effective and viable method for selectively converting lignocellulose into a liquid fuel—bio-oil. However, bio-oil derived from rapid pyrolysis contains a significant quantity of oxygen, which is dispersed in hundreds of oxygenates. These oxygenates are responsible for numerous undesirable qualities, including poor heating value, high corrosiveness, high viscosity, and instability; they also severely limit the use of bio-oil, notably as a transportation fuel. Because of their high energy density and compatibility with current infrastructure, hydrocarbons generated from biomass are particularly appealing. As a result, catalytic rapid pyrolysis has garnered a lot of attention for turning lignocellulose into transportation fuels. Many papers have been published on catalytic rapid pyrolysis of biomass. The fundamental problem of this process is the creation of active and stable catalysts capable of dealing with a wide range of lignocellulose breakdown intermediates. This review begins with an overview of the present state of knowledge in the chemistry of rapid pyrolysis of lignocellulose and then concentrates on the development of catalysts for catalytic fast pyrolysis. Recent experimental development in catalytic rapid pyrolysis of biomass is also discussed, with a focus on bio-oil yields and quality.[1]
The three main components of lignocellulosic biomass are cellulose, hemicellulose, and lignin. The production of active and stable catalysts capable of coping with a wide range of lignocellulose breakdown intermediates is the core difficulty of this procedure. We are exploring the chemistry of fast pyrolysis and the creation of catalysts in catalytic fast pyrolysis in this Yong Wang et al publication.[1]

The most abundant and least expensive carbon source is lignocellulosic biomass (such as wood, grass, and agricultural waste). As a result, it is a cost-effective and potentially carbon-neutral feedstock for the production of renewable biofuel. Bio-oil is the principal liquid product of fast pyrolysis of biomass, which is obtained by promptly quenching the pyrolysis gases. Bio-oils are made up of a wide range of condensable compounds that result from a series of simultaneous and sequential processes during the pyrolysis of lignocellulosic biomass. Bio-oil is a complex blend of over 300 oxygenated components. And, when compared to crude oil, bio oil produced through fast pyrolysis of woody biomass has a high oxygen content and H/C ratio. Because of the high water content (15-30%), biofuel has a low heating rate and flame temperature, a longer ignition delay, and a decreased combustion rate.

As a result, our key problem is reducing the oxygen concentration from biofuel in order to substitute diesel and gasoline.

Fast pyrolysis can be used to accomplish this. Catalytic Fast Pyrolysis is a catalyst that aids in the process (CFP). In general, two techniques have been applied during the last few decades: **catalytic cracking** and **hydrotreating.**[1]

Catalytic Cracking: At atmospheric pressure and without the need for hydrogen, catalytic cracking produces products with lower oxygen content than those produced by solid acid catalysts such as zeolites. However, it produces low-quality goods (benzene, toluene, and small chain alkane). As a result of its low carbon output and coke generation, as well as its short lifespan, it requires further refining.

Hydrotreating: It employs conventional fuel hydrotreating technologies to produce the desired product by eliminating oxygen from the hydrodeoxygenation process in a pressurised hydrogen atmosphere to break big molecules and employing catalysts such as supported molybdenum sulphide. Bio-oil hydrotreating has advanced and provides high-quality products.

However, because of the instability of bio-oil and the high oxygen content, it has a high running cost due to the necessity of some expensive catalysts and substantial hydrogen consumption.

Due to the short lifetime and low-quality products in cracking, as well as the high operating costs in hydrotreating, an alternate method is addressed in this paper: Catalytic Fast Pyrolysis (CFP), in which catalysts are immediately utilised in pyrolysis vapours before creating enhanced quality bio-oil.[1]

In the Fast Pyrolysis Process, two methods for mixing catalysts are addressed.

Ex-situ CFP: The catalyst is directly connected with pyrolysis fumes, resulting in higher quality bio-oil.

In-situ CFP: A catalyst is directly combined with the feedstock of a Pyrolysis Reactor in this method.[1]

2. Critical Review of the Literature

2.FAST PYROLYSIS PROCESS:

The fast pyrolysis of lignocellulose is accomplished by rapidly heating biomass to a moderate temperature in the absence of oxygen. Important factors include pyrolysis temperature, heating rate, residence period, and particle size. Having an impact on bio-oil production Increased residence time either increases gas phase or decreases gas phase. On char surfaces, pyrolysis vapour cracks or decomposes. The results of pyrolysis are separated into char, gases, and bio-oil. The ideal pyrolysis temperature was discovered to be around 500^{o}C, and the secondary reaction occurs either within or outside the Biomass particles. For big particles (>0.5 cm), intra-particle vapor-solid interactions are very relevant. For maximum bio-oil output, biomass particle size of 2 mm has been recommended.[1]

Previous efforts to understand the foundations of thermal pyrolysis of lignocellulose were mostly focused on the creation of global kinetic models with products utilising thermogravimetric and differential scanning calorimetry methods.

Thermogravimetric analysis (TGA) tests revealed that hemicellulose and cellulose pyrolysis happened swiftly. Hemicellulose decomposed mostly at 220-315^{o}C, whereas cellulose decomposed primarily at 315-400^{o}C. However, lignin is more difficult to breakdown, and weight loss occurred throughout a wide temperature range (160-900^{o}C), with substantial solid residue production.[1]

PYROLYSIS TECHNOLOGY:

	Process conditions			Products		
Pyrolysis technology	Residence time	Heating rate	Temperature (°C)	Char (%)	Bio-oil (%)	Gases (%)
Conventional	5–30 min	<50 °C min^{-1}	400–600	<35	<30	<40
Fast pyrolysis	<5 s	~1000 °C s^{-1}	400–600	<25	<75	<20
Flash pyrolysis	<0.1 s	~1000 °C s^{-1}	650–900	<20	<20	<70

Table 1. Comparison of three pyrolysis techniques

2.1.CHEMISTRY OF FAST PYROLYSIS:

Understanding the underlying characteristics of lignocellulosic biomass, as well as the chemistry of the processes occurring during rapid pyrolysis and CFP, is critical for rationally designing a more successful method.

Cellulose, hemicellulose, and lignin are the primary components of lignocellulosic biomass.

And the content of each component varies by biomass type. Woody biomass generally comprises 40-47 weight percent cellulose, 25-35 weight percent hemicellulose, and 16-31% weight percent lignin.

The most essential component of biomass is cellulose. It is available in both crystalline and amorphous forms. And the most majority of them are extremely crystalline, with polymeric degrees typically exceeding 9000.

Hemicellulose has a diverse composition and is structurally amorphous. Copolymers of five distinct C_5 and C_6 sugars, notably glucose, galactose, mannose, xylose, and arabinose, create it. Hemicellulose, unlike cellulose, is soluble in dilute alkali and has branching architectures that vary greatly amongst biomass resources.

Lignin is a three-dimensional polymer composed of propyl-phenol groups linked by ether and carbon-carbon linkages.[1]

2.2. FAST PYROLYSIS OF CELLULOSE:

Because of its abundance and simplicity of structure, cellulose is well investigated. The degree of crystallinity and crystallite diameters are the most critical parameters associated with cellulose's stability and reactivity. Each repeating unit has three hydroxyl groups, and the hydrogen bonds are either intramolecular or intermolecular, and they are connected to the conformation and stiffness of the single chain.

Fast The free radical process or the ionic mechanism is used in the pyrolysis of cellulose. Cellulose is converted into liquid before breakdown, and it decomposes in two ways.

One method is to directly produce tiny molecular products such as furan, levoglucosan, glycolaldehyde, and hydroxyl alcohols. Another advantage is that it produces low-degree oligomers, which can be further broken down into furan, light oxygenates, char, levoglucosan, and other compounds. Py-GCMS analysis identifies 27 chemicals. Furfural, levoglucosan, formic acid, acetic acid, and aldehyde compounds are the most important products.

Levoglucosan is produced as a liquid during cellulose pyrolysis, and part of it volatilizes to become a major volatile product. Condensed-phase secondary pyrolysis can also be used to produce pyrans and light oxygenates. Secondary decomposition of levoglucosan was discovered to be triggered by pyrolysis vapours produced from cellulose and lignin and hindered by xylan-derived vapour. Levoglucosan dehydration and isomerization result in the creation of additional anhydrous-monosaccharides. These anhydrous-monosaccharides can either re-polymerize to produce anhydrous-oligomers or be fragmented/retro-aldol condensation, dehydrated, de-carbonylation, or decarboxylated to form smaller oxygenates.

In CFP, Char is an undesirable Product. A substantial char yield is obtained from the subsequent reaction of initial pyrolysis products. Levoglucosan depolymerization and secondary pyrolysis were discovered to be significant routes for char production. Increased residence time results in increased char production due to secondary reaction yield in primary pyrolysis products.[1]

2.3. FAST PYROLYSIS OF REACTIVE GAS:

Fast pyrolysis is often performed in the absence of oxygen, using nitrogen as a carrier gas.
Similarly, H_2, CO_2, CO, CH_4, and oxidative atmosphere have been studied to varying degrees. Water is a significant component of lignocellulose biomass. Steam promotes wood decomposition and reduces activation energy. Steam improves heat transfer due to the desorption of steam on low molecular weight products, resulting in the highest yield.
Another significant benefit of the stem is a 30-45% reduction in coke formation. It decreases coke formation in the presence of a hydrogen atmosphere, but has no influence on gas yield or

liquid yield composition. When a hydro-processing catalyst, such as Supported Molebdnum, is added to it. Catalytic Hydro-processing leads to higher Bio-oil yield and reduction in oxygen content. It is decreased by about 16% less than without a catalyst. When we further increase the temperature to 500-650^{o}C. It further removes the oxygen content. However, at 300^{o}C it shows the minimal effect on bio-oil

It was discovered that the CO atmosphere has the lowest liquid yield (49.6%), but the CH_4 atmosphere has a greater liquid yield (58.7%). The highest CO_2 and H_20 conversion rates were recorded in the CO and H_2 atmospheres. When CO and CO_2 were used as carrier gases, less methoxyl-containing compounds and more monofunctional phenols were discovered.

Syngas has been discovered to be a viable alternative to pure hydrogen in coal hydro-pyrolysis. Because the weight loss curve for both hydrogen and syngas was seen to be the same. This suggests that syngas might replace hydrogen as the Pyrolysis medium. CFP might combine rapid pyrolysis with various chemical processes for vapour upgrading into a simple process that could create high-quality, low-cost bio-oils.[1]

For modelling of biomass pyrolysis, three distinct scales are crucial: the molecular, particle, and reactor sizes. For the creation of a multi-scale model in the future, molecular-level research elaborates the mechanism of biomass pyrolysis through the main and secondary pyrolysis events. As demonstrated in Figure 1, lumped kinetic models connected to reactors, and entire network models may aid in understanding heat, mass, and species movement at particle scales, and mechanistic models give insight into reaction processes at the molecular level.[2]

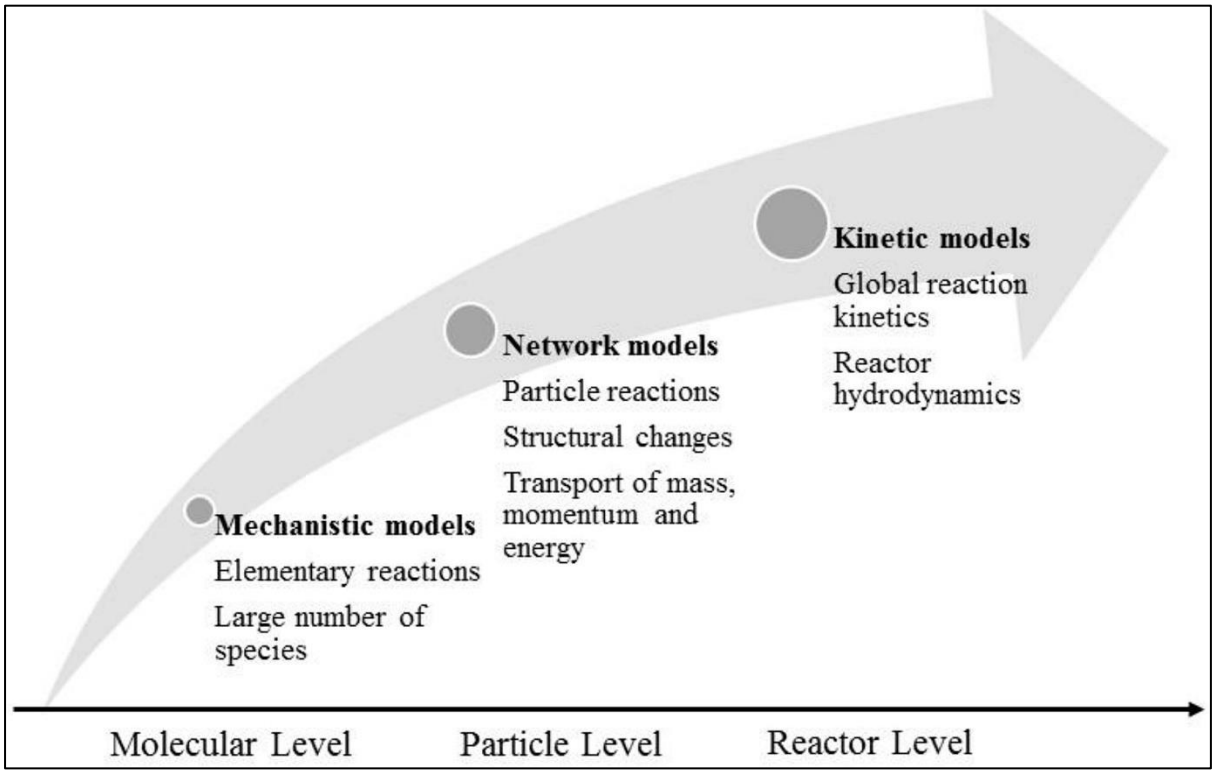

Figure 1. Different levels of modelling for biomass pyrolysis [2]

3. Methodology

Conversion of biomass to energy takes place via two pathways: thermochemical and biological methods. Pyrolysis is not only efficient Thermochemical way for conversion but the first preceding Process of another thermochemical process such as gasification, liquefaction, carbonization, and combustion.

The non-isothermal analysis is a dynamic method used to analyze biomass pyrolysis. Thermogravimetric analysis (TGA) is used for data collecting with different heating rates for model fitting which determines kinetic triplets that is Activation Energy, frequency factor, and reaction mechanism.

Understanding kinetics is a key step to Pyrolysis Technology, without deep learning of kinetics it is impossible to build the reactor model.

Kinetic models have been developed in recent years and is classified into five models.

1. One-step global kinetic model based on model fitting

A one-step global model is used to describe the pyrolysis of cellulose through a first-order irreversible reaction from which apparent activation energy is obtained. It shows good performance for the kinetics of cellulose but for the complex composition of biomass it can't be used because of its complexity.

2. Global model based on the model-free method

A global model based on a model-free method does not need any prior assumptions. This model obtains accurate kinetic parameters based on data collected from thermogravimetric under different heating rates.

3. Multistep successive model

Multi-step successive models work as similar to one-step global model analyses kinetics of biomass. It splits biomass pyrolysis into phases based on temperature and mass loss, then calculates kinetics parameters based on these stages.

4. Semi-global model

Semi global model is more complicated than the multi-step model because it involves several solid phase reactions and some reactions of tar and gases. Kinetic reaction obtained by semi-global model is more detailed because it considers reaction mechanisms.

5. Distributed activation energy-based model (DAEM)

Distributed activation energy model is based on semi global model which assumes that infinite, independent, parallel reaction compose the pyrolysis process, and their activation energy is described by continuous probability function. DAEM recently employed to analyse kinetics of coal and complex biomass.[3]

Most of studies focuses on kinetics of biomass pyrolysis but there is very less research on kinetics of catalytic biomass pyrolysis. Many researchers studied influence of catalyst on gasification performance and bio-oil from biomass. Recent research has discovered that the multifunctional material Ni-$CaOCa_2SiO_4$ improves biomass gasification performance.

However, kinetics performance of biomass Pyrolysis is not systematically investigated. So, in order to understand progress biomass catalyst pyrolysis study aims to employ DAEM to analyse the kinetics of biomass and obtains the kinetic parameters. And by the help of TG-MS analysis, the effects of functional material on products and kinetics of catalytic biomass pyrolysis have been further investigated.[3]

Materials:

Biomass Feedstock:

Straw, sawdust, and cellulose were selected for the study. Before carrying out the sample it is milled and sieved into powder with a diameter of 180 μm. And then this sieved sample is dried at 105^0C for 12h. after drying carbon, hydrogen, oxygen, nitrogen, and sulfur were measured using Elemental Analyzer and sulfur Analyzer. And proximate analysis includes volatile matter, fixed carbon and ash content.[3]

3.1. Functional Materials:

For the study Ni-CaO-Ca_2SiO_4 and Ni-Ca_2SiO_4 are the functional material. Where Ni acts as catalyst in cracking C-C, C-H and O-H Bonds. CaO is CO_2 Sorbent to shift reforming reaction towards H_2 direction. $CaSiO_4$ works as a stabilizer to Combat material sintering and it does not absorb CO_2. Synthesis of functional material done by freeze-drying, calcination, and reduction synthesis. Ni content in Ni-CaO-Ca_2SiO_4 and Ni-Ca_2SiO_4 were 20 wt% in both.

3.2.TG-MS experiment

Pyrolysis experiments were conducted using Thermogravimetric mass spectrometry (TG-MS). MS is directly connected to the TGA outlet with a heated connection to avoid condensation of products. For comparison purposes, biomass pyrolysis is also done without catalyst, using a 4-5mg sample. For biomass pyrolysis with functional material carried out by equal percentage biomass and functional material around 6-7 mg mixture of sample is used. Before starting the process, argon flow was used to clean the furnace of TGA to eliminate air interference. Then furnace was heated up to 100^0C at a heating rate of 10^oC/min and kept it for 10 min to remove moisture from the Biomass.

For kinetic analysis, mass loss of pyrolysis is measured using different heating rates of 20,30,40, and 50 ^{o}C/min from 100^{o}C to 800^{o}C in argon flow rate of 500 ml/min. mass/charge signals were recorded at 2,15,18,28,28,40,44 by MS which represent corresponding gases H_2, CH_4, H_2O, CO, Ar, and CO_2. The gas products were determined through a semi-quantitative method from the signals of Argon flow.[2]

3.3. Kinetic Analysis[10]:

During the pyrolysis process, the reaction rate is expressed as,

$$\frac{d\alpha}{dz} = k(T)f(\alpha) \tag{1}$$

k(T) = reaction rate constant, α is conversion rate constant, f(α) is reaction model which depends upon reaction mechanism.

we can determine k(T) by using the Arrhenius equation as follows,

$$\mathrm{k(T)} = -\mathrm{k_o}\exp\left(-\frac{\mathrm{E}}{\mathrm{RT}}\right) \tag{2}$$

K_o, E, R, and T are frequency factor(min^{-1}), activation energy (kJ/mol), universal gas constant, and Temperature(K),

During non-isothermal TGA Process, heating rate is,

$$\beta = \frac{\mathrm{dT}}{\mathrm{dt}} \tag{3}$$

From Equation (1), (2) and Equation (3), we obtain Equation (4),

$$\frac{\mathrm{d}\alpha}{\mathrm{dT}} = \frac{\mathrm{k_o}}{\beta}\exp\left(-\frac{\mathrm{E}}{\mathrm{RT}}\right)\mathrm{f}(\alpha) \tag{4}$$

After integration, we obtain equation (5)

$$\mathrm{G}(\alpha) = \int_0^{\mathrm{T}} \exp\left(-\frac{\mathrm{E}}{\mathrm{RT}}\right)\mathrm{dT} \tag{5}$$

In study of apparent activation energy E, was compared with different methods:

3.4. Kissinger-Akahira-Sunose (KAS) method[4]:

By integrating equation (5), we get equation (6)

$$\ln\frac{\beta}{\mathrm{T}^2} = \ln\frac{\mathrm{R} * \mathrm{k_0}}{\mathrm{EG}(\alpha)} - \frac{\mathrm{E}}{\mathrm{RT}} \tag{6}$$

four pairs of $\ln\left(\frac{\beta}{T^2}\right)$ and $1/T$ data points were plotted at different heating rates and E is estimated from slope.

3.5. Flynn-Wall-Ozawa Method(FWO)[5]:

Using equation (5) and Doyle's Approximation we get equation (7)

$$ln\beta = ln\frac{0.0048AE}{RG(\alpha)} - 1.052\frac{E}{RT} \tag{7}$$

Temperature T and Conversion α measured from TGA experiments. By plotting $\ln\beta \ vs \ 1/T$ at same conversion and different heating rates β, E can be estimated.

3.6.Starink method[6]**:**

By analysing equation (6) and (7) and using approximations of Temperature integral, we get this equation

$$ln\frac{\beta}{T^{1.92}} = C_s - 1.0008\frac{E}{RT} \quad (8)$$

By plotting ln $(\frac{\beta}{T^{1.92}})$ $vs\ 1/T$ at same conversion and different heating rates β, E can be estimated.

3.7. Distributed Activation Energy Model[7]**:**

In Biomass Pyrolysis experiments, DAEM Model used to determines kinetics of complex reaction. It assumes that it is composed of large number of independent First-order parallel reaction with different activation energies and frequency factor. Difference between activation energies is defined as activation energy function f(E). this method employed to analyse kinetics and obtained parameters
E and K_o.

Final Expression for DAEM is as follows:

$$ln\frac{\beta}{T^2} = ln\left(\frac{Rk_0}{E}\right) + 0.6075 - E/RT \quad (9)$$

we get Arrhenius plot by plotting points ln $(\frac{\beta}{T^2})$ and $1/T$, E and Ko are estimated by slope and intercept.

3.8. Friedman model (FM) [8]**:**

FM is a differential model. It has given more accurate results than KAS and FWO. The quote from Friedman is as follows

$$\text{Ln}(\beta\frac{d\alpha}{dt}) = \ln(K_o f(\alpha)) - \frac{E_a}{RT} \quad (10)$$

From graph between $ln(\beta\frac{d\alpha}{dt})$ vs $\frac{1}{T}$ at a constant conversion value, activation energy is determined using slope $(-\frac{E_a}{R})$

3.9.Master Plot[9]**:**

Although model-free methods were considered to be more reliable, the activation energy was the only parameter can be calculated. Whereas model-fitting methods took the reaction mechanism function into consideration, and more kinetic parameters can be obtained, such as pre-exponential factor A and the fittest reaction mechanism function f(α).

The z(α) plots are derived by combining the integral and differential forms of reaction model

The reaction model's integral and differential forms are combined to create the z(α) graphs.

$$Z(\alpha) = f(\alpha) * g(\alpha)$$

$$Z(\alpha) = \frac{d\alpha}{dt} \exp\left(\frac{E_\alpha}{RT_\alpha}\right) \int_0^{T_\alpha} \exp\left(\frac{-E_a}{RT}\right) \quad (11)$$

By using the fourth rational expression of the Senum-Yang approximation, the temperature integral is roughly calculated. In comparison to the Senum-Yang approximation, the temperature integral solved using the trapezoidal rule produces fewer errors, demonstrating that the Senum-Yang approximation produces accurate results with less computation. The best fit model is chosen after comparing the theoretical and experimental z(α) curves. The pre-exponential factor is additionally ascertained from any of the integral or differential rate specified Expression.

Mechanism	Symbol	f(α)	g(α)
Diffusion Models			
1D diffusion	D1	$1/(2\alpha)$	α^2
2D diffusion (Valensi model)	D2	$[-\ln(1-\alpha)]^{-1}$	$(1-\alpha)\ln(1-\alpha)+\alpha$
3D diffusion (Jander model)	D3	$3/2(1-\alpha)^{2/3}[1-(1-\alpha)^{1/3}]^{-1}$	$[1-(1-\alpha)^{1/3}]^2$
3D diffusion (Ginstling model)	D4	$3/2[(1-\alpha)^{1/3}-1]^{-1}$	$1-2/3\alpha-(1-\alpha)^{2/3}$
Nucleation Models			
Power law	P2	$2/3\alpha^{-1/2}$	$\alpha^{3/2}$
Power law	P3	$2\alpha^{1/2}$	$\alpha^{1/2}$
Power law	P4	$3\alpha^{2/3}$	$\alpha^{1/3}$
Power law	P5	$4\alpha^{3/4}$	$\alpha^{1/4}$
Sigmoidal Rate Equations			
Avrami-Erofeev	A1	$1/2(1-\alpha)[-\ln(1-\alpha)]^{1/3}$	$[-\ln(1-\alpha)]^{2/3}$
Avrami-Erofeev	A2	$2(1-\alpha)[-\ln(1-\alpha)]^{1/2}$	$[-\ln(1-\alpha)]^{1/2}$
Avrami-Erofeev	A3	$3(1-\alpha)[-\ln(1-\alpha)]^{2/3}$	$[-\ln(1-\alpha)]^{1/3}$
Avrami-Erofeev	A4	$4(1-\alpha)[-\ln(1-\alpha)]^{3/4}$	$[-\ln(1-\alpha)]^{1/4}$
Contracting cylinder	F2	$2(1-\alpha)^{1/3}$	$1-(1-\alpha)^{1/2}$
Contracting sphere	F3	$(1-\alpha)^{2/3}$	$1-(1-\alpha)^{1/3}$
Random nucleation	F4	$(1-\alpha)^2$	$1/(1-\alpha)$
Reaction order Models			
1st-order	R1	$(1-\alpha)$	$[-\ln(1-\alpha)]$
2nd-order	R2	$(1-\alpha)^2$	$(1-\alpha)^{-1}-1$
3rd-order	R3	$(1-\alpha)^3$	$1/2[(1-\alpha)^{-2}-1]$
$1^{1/2}$ order	R6	$(1-\alpha)^{3/2}$	$2[(1-\alpha)^{-1/2}-1]$

Table 2. Expressions for f(α) and g(α) functions for solid state reactions[10]

TGA information acquired from a paper:

Biomass	conditions	(20)	(30)	(40)	(50)	Peak
Straw	without catalyst	522.56- 718.04	529.37-727.35	532.99-729.24	537.02-733.05	595.16
	with Ni-$CaOSi_2O_4$	527.42-892.85	533.47-910.19	538.02-917.99	541.90-929.36	588.69
	with Ni-Ca_2SiO_4	524.34-829.17	529.60-842.40	533.62-850.358	537.23-855.01	582.36
Sawdust	without catalyst	549.93-698.6	556.60-704.4	562.45-710.69	566.17-714.28	644.79
	with Ni-$CaOSi_2O_4$	557.52-880.41	565.41-895.83	570.81-908.315	574.81-574.92	648.74
	with Ni-Ca_2SiO_4	551.30-756.66	559.15-772.26	563.51-787.85	567.58-789.9	650.84
Cellulose	without catalyst	590.77-640.08	597.65-648.43	603.18-654.94	607.75-661.03	624.67
	with Ni-$CaOSi_2O_4$	595.27-738.92	602.42-802.19	608.18-827.72	611.32-864.81	620.47
	with Ni-Ca_2SiO_4	592.20-651.19	599.71-659.71	605.86-666.60	608.96-674.02	628.22

Table 3. data for Biomass Straw, Sawdust and Cellulose 1)without catalyst, 2)with Ni-$CaOSi_2O_4$ Catalyst 3)with Ni-Ca_2SiO_4 Catalyst 2) Sawdust without Catalyst

The temperature at four distinct heating rates (β) i.e.20,30,40,50^oC/Min. with varied conversion factors ranging from 0.05 to 0.9 for three kinds of biomass are shown by the data above. With three conditions, straw, sawdust, and cellulose 1) Without Catalyst 2)With Ni-$CaOSi_2O_4$ Catalyst 3) with Catalyst Ni-Ca_2SiO_4

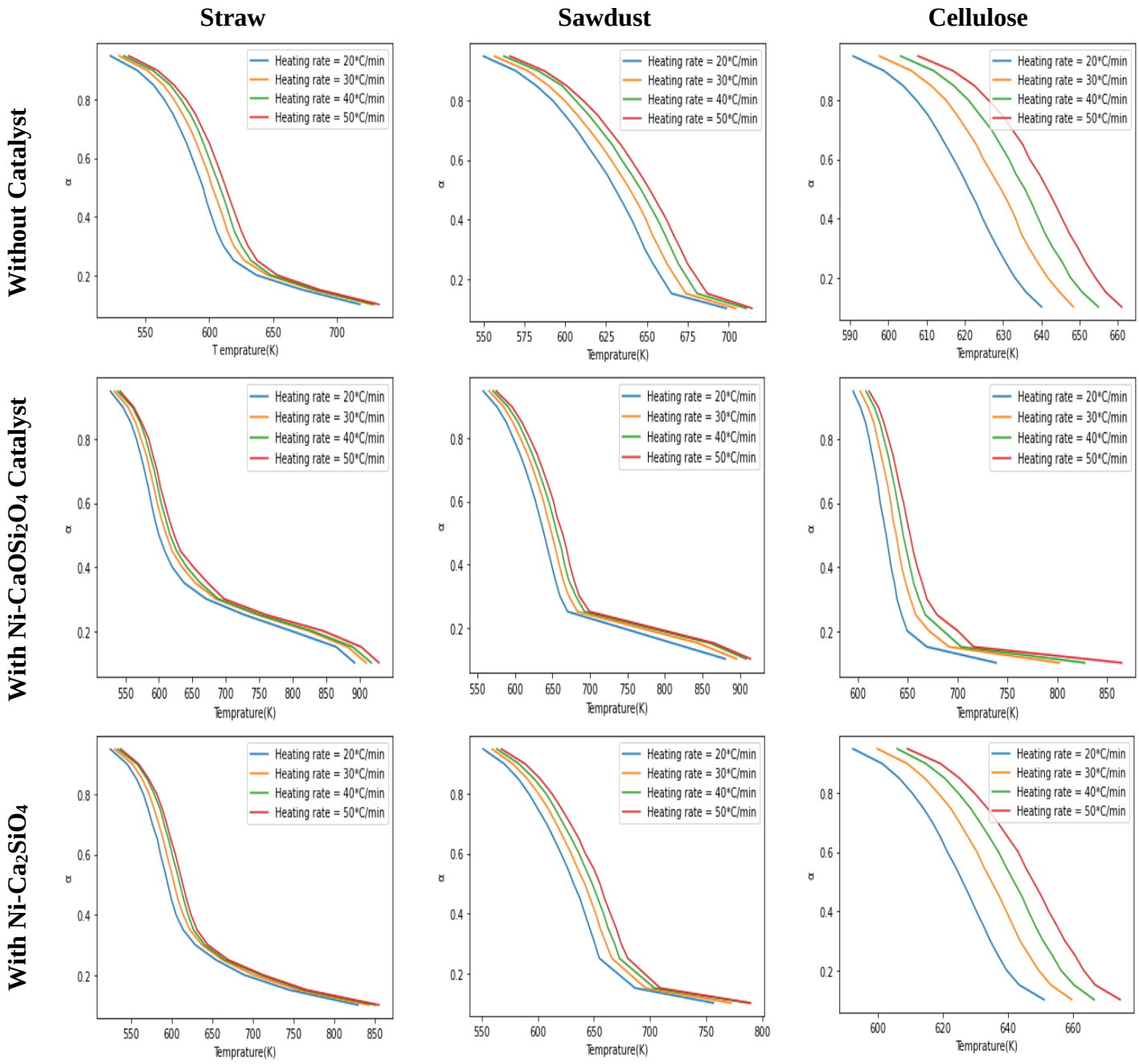

Figure 2.Temprature curves of Straw, Sawdust and Cellulose Biomass under Three Condition 1) With Catalyst 2) With Ni-CaO-Si_2O_4 Catalyst 3) With Ni-Ca_2SiO_4 with different Heating rates

4. Results and Discussions:

4.1.Straw without Catalyst:

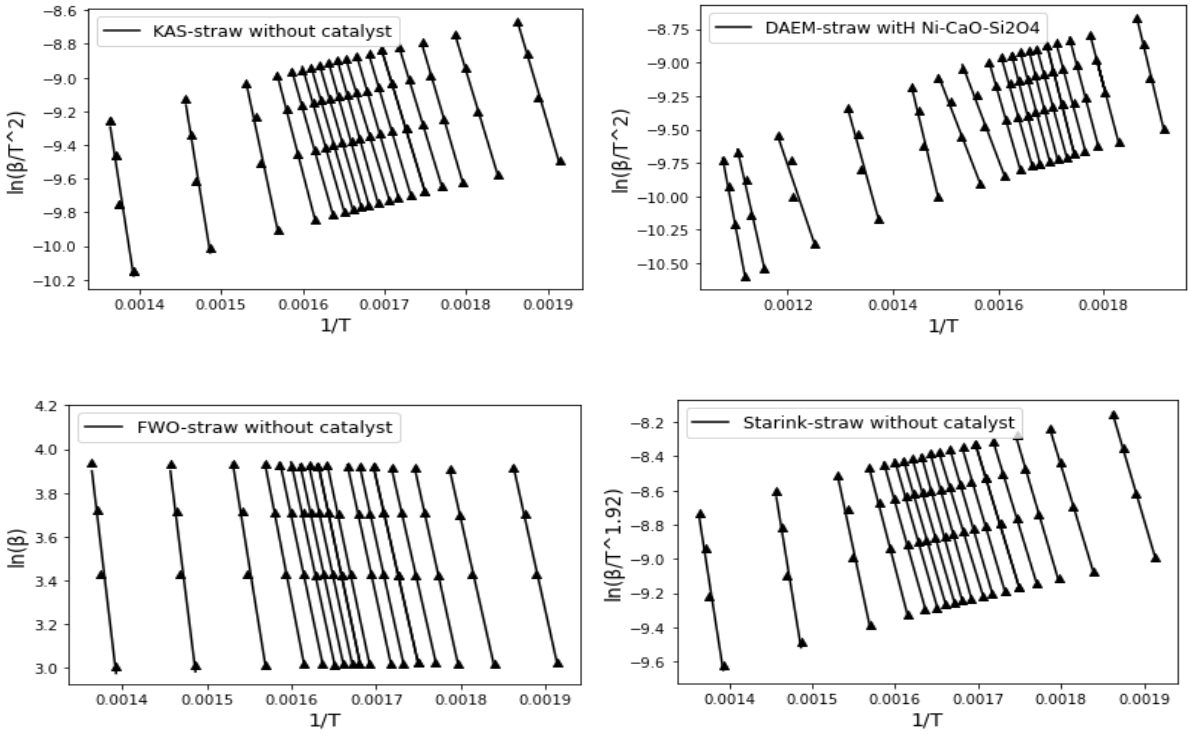

Figure 3.Arrhenius plot of Straw at different degrees from: (a) DAEM ,(b)FWO ,(c) KAS, (d) Starink methods

The Kinetics of straw biomass were determined by using 4 model free iso conversion Methods at a degree of freedom ranging from 0.05 to 0.9 showed in above figure. Arrhenius plot for straw without catalyst at different degrees derived from 1) KAS, 2) DAEM, 3)FWO, 4)Starink methods, where arrows in each lines defines different heating rates varying from 20 to 50^{o}C/min. and each lines from Right to left Defines different degrees of freedom from 0.05 to 0.9.

Activation energy, overall correlation(R^2) and frequency defined from various methods at different degrees of freedom is defined below Table. Overall correlation (R^2) is above 0.9, which signifies that all the methods is suitable for modelling.

Straw's activation energy without a catalyst range from 134 to 187 KJ/mol. At conversion stages 0.85-0.9, it demonstrated a high activation energy of 230-252 KJ/mol. As conversion increases, the pre-exponential factor gradually increases.

	DAEM			KAS		
α	**R^2**	**E_a**	**K_o**	**R^2**	**E_a**	**K_o**
0.05	0.9979	141.13	1.6E+13	0.9979	141.13	1.5E+13
0.1	0.9977	136.71	1.5E+12	0.9977	136.71	1.4E+12
0.15	0.9973	139.3	1.3E+12	0.9973	139.3	1.2E+12
0.2	0.9998	135.6	3.5E+11	0.9998	135.6	3.3E+11
0.25	0.9996	134.82	2.1E+11	0.9996	134.82	1.9E+11
0.3	0.9991	137.92	3E+11	0.9991	137.92	2.8E+11
0.35	0.9998	139.91	3.5E+11	0.9998	139.91	3.3E+11
0.4	0.9994	133.95	8.1E+10	0.9994	133.95	7.5E+10
0.45	0.9996	143.92	5.2E+11	0.9996	143.92	4.8E+11
0.5	0.9994	145.38	5.7E+11	0.9994	145.38	5.4E+11
0.55	0.9996	138.96	1.3E+11	0.9996	138.96	1.2E+11
0.6	0.9993	140.12	1.3E+11	0.9993	140.12	1.2E+11
0.65	0.9991	140.61	1.2E+11	0.9991	140.61	1.1E+11
0.7	0.9997	142.9	1.5E+11	0.9997	142.9	1.4E+11
0.75	0.9995	155.21	1.2E+12	0.9995	155.21	1.1E+12
0.8	0.9864	187.14	2.4E+14	0.9864	187.14	2.2E+14
0.85	0.9909	231.21	1.2E+17	0.9909	231.21	1.1E+17
0.9	0.9747	252.79	2.8E+17	0.9747	252.79	2.6E+17

	FWO			Friedman		
α	**R^2**	**E_a**	**K_o**	**R^2**	**E_a**	**K_o**
0.05	0.9982	142.52	2.2E+13	0.9979	137.91	1.7E+17
0.1	0.998	138.66	2.3E+12	0.9966	138.28	6.9E+16
0.15	0.9976	141.33	2E+12	0.9994	136.26	3.5E+16
0.2	0.9998	137.96	6.1E+11	0.9978	131.11	9.9E+15
0.25	0.9997	137.33	3.7E+11	0.9984	140.53	6.6E+16
0.3	0.9992	140.36	5.2E+11	0.9984	147.98	2.9E+17
0.35	0.9999	142.34	6.1E+11	0.9987	126.77	3E+15
0.4	0.9995	136.73	1.5E+11	0.9968	139.01	3.4E+16
0.45	0.9996	146.28	8.8E+11	0.9921	169.37	1.5E+19
0.5	0.9995	147.73	9.7E+11	0.9948	127.05	2.2E+15
0.55	0.9996	141.69	2.3E+11	0.9748	122.35	7.1E+14
0.6	0.9994	142.85	2.4E+11	0.9884	145.24	6.5E+16
0.65	0.9992	143.38	2.3E+11	0.9925	146.47	6.1E+16
0.7	0.9997	145.64	2.8E+11	0.9992	161.35	6.6E+17
0.75	0.9995	157.46	1.9E+12	0.9934	189.89	7.2E+19
0.8	0.9878	188.09	2.8E+14	0.9756	220.06	4.2E+21
0.85	0.9917	230.5	1.1E+17	0.9903	248.11	5.1E+22
0.9	0.9768	251.76	2.3E+17	0.9695	261.7	2.5E+22

Table 4. Activation Energy(Ea(kJ/mol)) and Pre-exponential Factor, calculated from 4 Methods i.e. DAEM KAS, FWO and Friedman Straw without catalyst

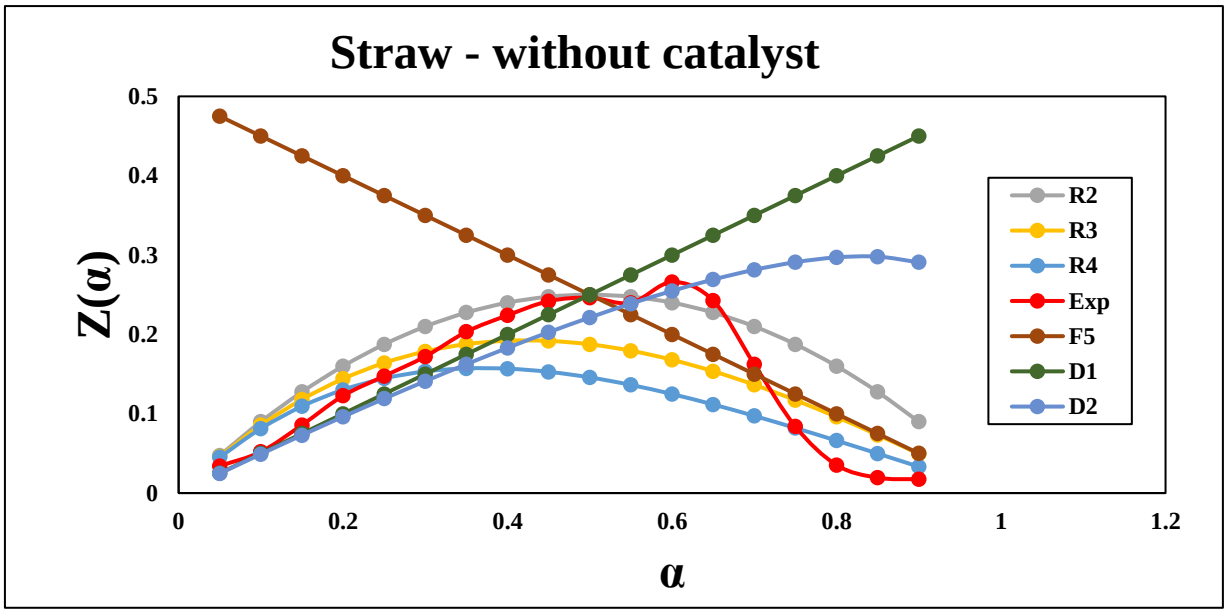

Figure 4. Master plot for Straw - without catalyst

This pyrolysis process appears to be diffusion-controlled for conversion regions ranging from 5% to 15% for straw without a catalyst condition. From conversion, 20% predicted 4th order reaction, then order continues to decrease as conversion increases, eventually reaching second order. The experimental master plot was closer to the three-dimensional Jander equation at 55%, and it predicted values closer to the random nucleation reaction model at 70%. Overall, master plots revealed that second order (R2) and diffusion controlled random nucleation reaction mechanisms dominate pyrolysis of straw biomass with No Catalyst.

.

4.2.Straw - with $NiCaOSi_2O_4$ catalyst:

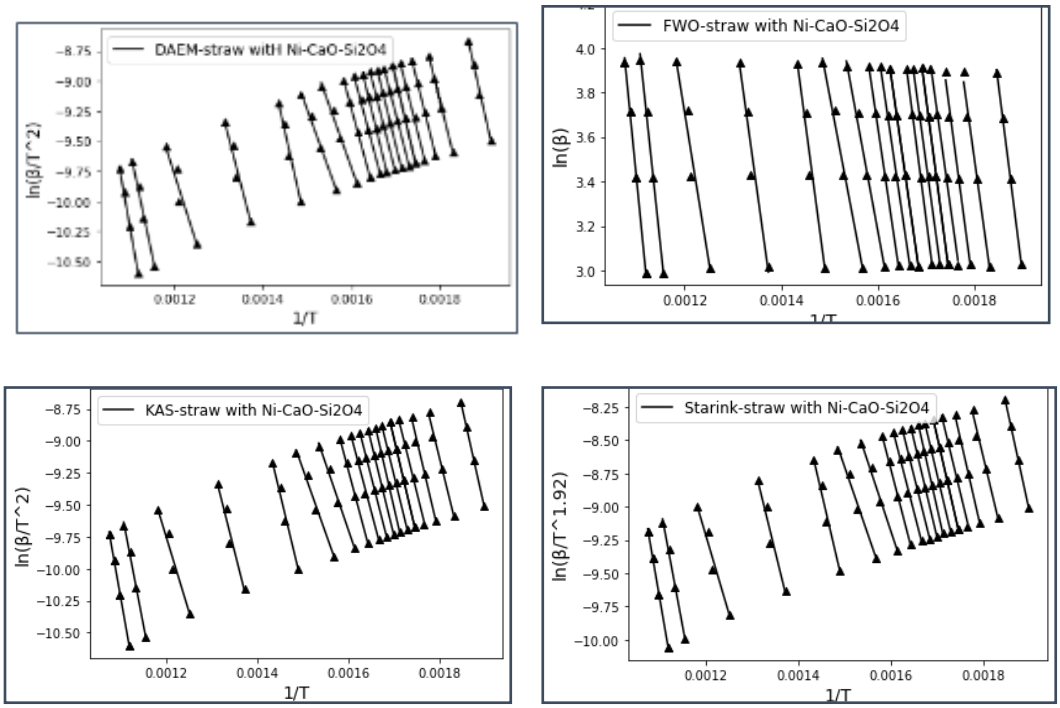

Figure 5.Arrhenius plot of straw with Ni-CaO-Si_2O_4 catalyst at different degrees from: (a) DAEM,

The kinetics of straw biomass were determined using four model free iso conversion methods with degrees of freedom ranging from 0.05 to 0.9, as shown in the figure above. Arrhenius plot for straw with $NiCaOSi_2O_4$ catalyst at various degrees derived from 1) KAS, 2) DAEM, 3)FWO, and 4)Starink methods, with arrows in each line defining different heating rates ranging from 20 to 50^{o}C/min and each line running from right to left. Defines various degrees of freedom ranging from 0.05 to 0.9.

The activation energy, overall correlation (R^2), and frequency defined by various methods at various degrees of freedom are defined in the table below. The overall correlation (R^2) is greater than 0.9, indicating that all of the methods are suitable for modelling.

Straw activation energy with Ni-$CaOSi_2O_4$ catalyst ranges from 88 to 161 kJ/mol. And as the number of conversion stages increased, the activation energy decreased, but at the final stages, it increased to 148-170 kJ/mol. Which is less than without the catalyst condition, and the pre-exponential factor decreases gradually as conversion increases.

	DAEM			KAS		
α	**R^2**	**E_a**	**K_o**	**R^2**	**E_a**	**K_o**
0.05	0.9995	141.82	1.4E+13	0.9995	141.82	1.3E+13
0.1	0.9921	136.68	1.2E+12	0.9921	136.68	1.1E+12
0.15	0.9923	133.15	2.9E+11	0.9923	133.15	2.7E+11
0.2	0.9916	125.22	3.4E+10	0.9916	125.22	3.2E+10
0.25	0.9992	132.88	1.3E+11	0.9992	132.88	1.2E+11
0.3	0.9995	128.15	3.4E+10	0.9995	128.15	3.2E+10
0.35	0.999	134.87	1.1E+11	0.999	134.87	1E+11
0.4	0.9996	127.18	1.7E+10	0.9996	127.18	1.6E+10
0.45	0.9991	119.7	2.7E+09	0.9991	119.7	2.5E+09
0.5	0.9967	115.54	8.7E+08	0.9967	115.54	7.9E+08
0.55	0.999	114.35	4.8E+08	0.999	114.35	4.3E+08
0.6	0.9951	88.38	1550616	0.9951	88.38	1364595
0.65	0.9939	83.33	328276	0.9939	83.33	284799
0.7	0.979	123.94	2.9E+08	0.979	123.94	2.6E+08
0.75	0.9688	117.65	1.4E+07	0.9688	117.65	1.3E+07
0.8	0.9718	96	69115.3	0.9718	96	58696.8
0.85	0.9916	148.17	4.2E+07	0.9916	148.17	3.8E+07
0. 9	0.9946	161.77	1.4E+08	0.9946	161.77	1.3E+08

	FWO			Friedman		
α	**R^2**	**E_a**	**K_o**	**R^2**	**E_a**	**K_o**
0.05	0.9996	143.26	1.9E+13	0.9948	139.69	5.8E+15
0.1	0.9931	138.7	1.8E+12	0.9862	131.91	4.3E+14
0.15	0.9932	135.52	5.2E+11	0.9891	120.67	3.1E+13
0.2	0.9927	128.12	6.9E+10	0.9966	131.86	3.2E+14
0.25	0.9993	135.51	2.3E+11	0.9896	133.83	4.2E+14
0.3	0.9996	131.11	6.9E+10	0.9967	135.72	5.2E+14
0.35	0.9991	137.57	2E+11	0.9958	134.6	3.5E+14
0.4	0.9996	130.35	3.6E+10	0.9886	98.59	1.4E+11
0.45	0.9992	123.33	6.5E+09	0.9843	99.2	1.1E+11
0.5	0.9972	119.49	2.3E+09	0.9899	106.49	3.3E+11
0.55	0.9992	118.5	1.3E+09	0.9997	89.39	5.1E+09
0.6	0.9961	94.05	7044844	0.9669	58.53	4381310
0.65	0.9952	89.56	1740543	0.9897	95.98	3.5E+09
0.7	0.9822	128.62	8.2E+08	0.9711	160.67	1.4E+14
0.75	0.9742	123.58	5.1E+07	0.9636	110.41	1.7E+09
0.8	0.9781	104.21	420000	0.9852	110.05	3.1E+08
0.85	0.9931	154.81	1.4E+08	0.9976	174.24	1.8E+12
0.9	0.9955	168.17	4.1E+08	0.9971	181.67	3.3E+12

Table 5. Activation Energy(Ea(kJ/mol)) and Pre-exponential Factor, 4 Methods i.e. DAEM KAS, FWO and Friedman Straw with $NiCaOSi_2O_4$ Catalyst

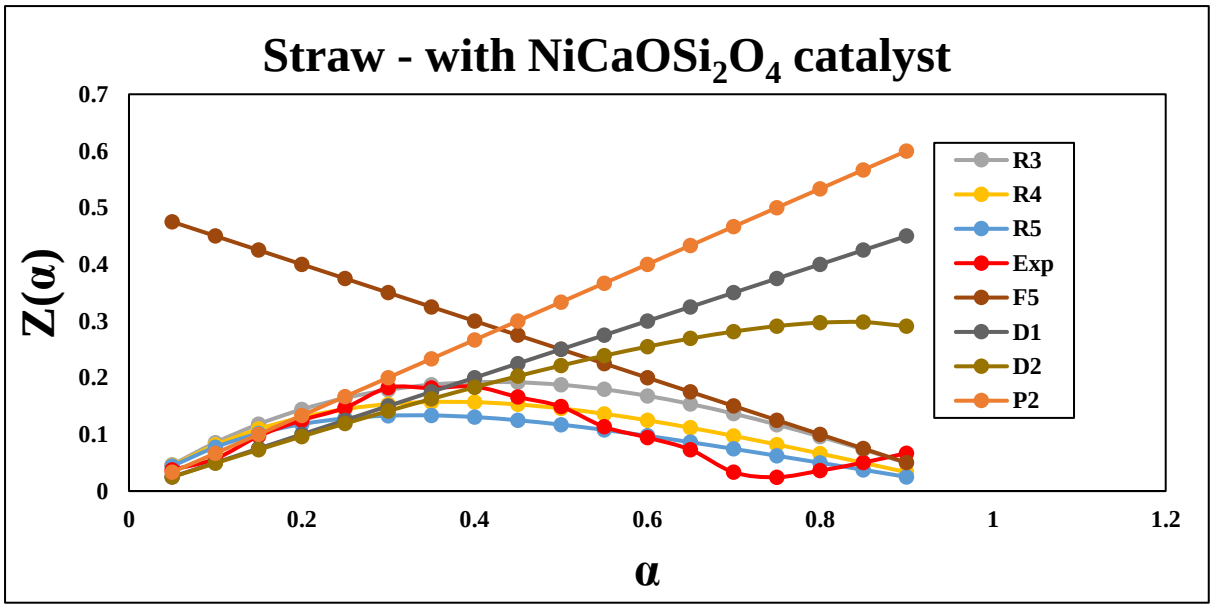

Figure 6. Master plot for Straw - with $NiCaOSi_2O_4$ catalyst

The master plot is utilised to establish the reaction mechanism; for straw with $NiCaOSi_2O_4$ catalyst, originally 20% conversion followed the Nucleation power model and 5^{th} order reaction order was seen; however, it began to drop order 5^{th} order to between half order and third order. The reaction is regulated by a diffusion-controlled mechanism between conversions of 35% and 40%. And the conversion order of the reaction increased from third to fifth order, from 45% to 65%. At the end of the reaction, the order of the reaction gradually decreases from 5th order to 3rd order to half order. This is because to the numerous reaction pathways that occur during the thermal degradation of Straw with $NiCaOSi_2O_4$.

In a nutshell, master plots revealed that pyrolysis of straw biomass with $NiCaOSi_2O_4$ Catalyst is majorly governed by 5^{th} order (R5) and third-order (R3) with nucleation reaction and Diffusion controlled mechanisms. This shows that the use of $NiCaOSi_2O_4$ Catalyst altered the reaction mechanism, which is helpful to produce targeted biofuels

4.3.Straw - $NiCa_2SiO_4$ catalyst:

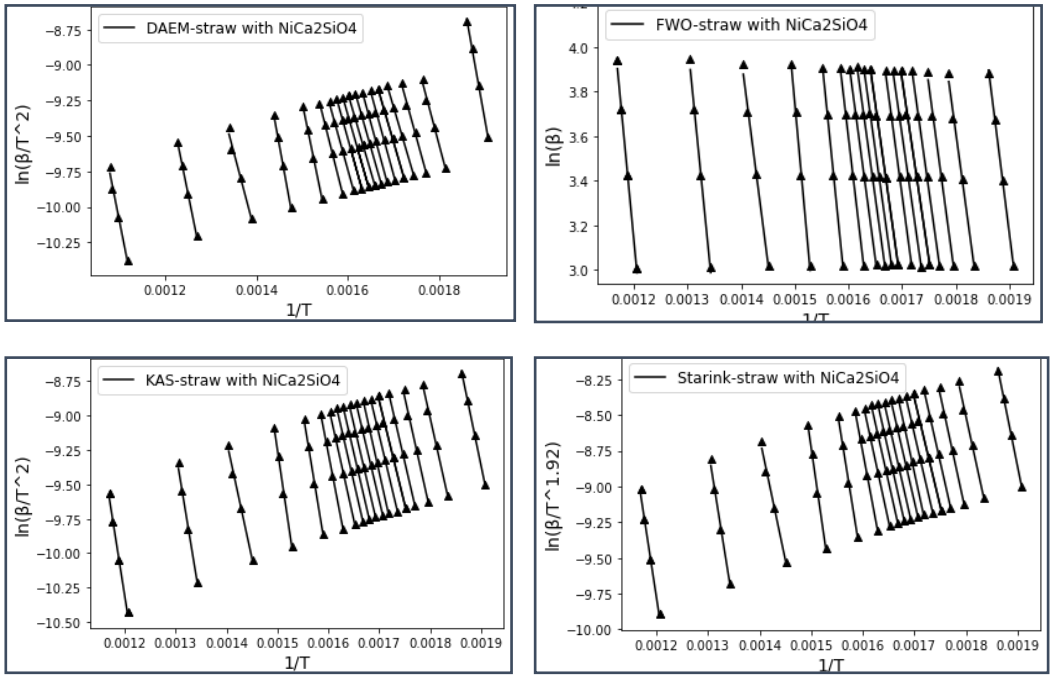

Figure 7. Arrhenius plot of straw with Ni-Ca_2SiO_4 catalyst at different degrees from
(a) DAEM, (b) FWO,(c) KAS (d) Starink methods

The kinetics of straw biomass were calculated using four model free iso conversion methods with degrees of freedom ranging from 0.05 to 0.9, as shown in the figure above. Arrhenius plot for straw with $NiCa_2SiO_4$ catalyst at various degrees generated from 1) KAS, 2) DAEM, 3)FWO, and 4)Starink techniques, with arrows in each line defining different heating rates ranging from 20 to 50°C/min with each line running from right to left. Defines several degrees of freedom ranging from 0.05 to 0.9.

The activation energy, overall correlation (R^2), and frequency determined by various approaches at various degrees of freedom are defined in the table below. The overall correlation (R^2) is more than 0.9, indicating that all of the approaches are adequate for modelling.

Straw activation energy with Ni-Ca_2SiO_4 catalyst ranges from 130 to 200 kJ/mol. And as the conversion phases progressed, it revealed variable activation energy that was steadily rising, reaching 183-205 kJ/Mol at the last stages. Which is less than the condition without the catalyst but greater than the condition with the $NiCaOSi_2O_4$ catalyst, and the pre-exponential factor gradually decreases as conversion increases.

	DAEM			KAS		
α	**R^2**	**E_a**	**K_o**	**R^2**	**E_a**	**K_o**
0.05	0.999	158.51	8.7E+14	0.999099	158.5164	8.3E+14
0.1	0.9932	144.58	8.3E+12	0.993292	144.5805	7.8E+12
0.15	0.9932	144.37	3.9E+12	0.993264	144.378	3.6E+12
0.2	0.9978	137.99	5.9E+11	0.997886	137.9961	5.5E+11
0.25	0.9919	145.86	2.3E+12	0.991996	145.8629	1.6E+12
0.3	0.9914	137.4	3.7E+11	0.991485	137.4022	4.1E+11
0.35	0.996	145.62	1.2E+12	0.996021	145.6205	1.1E+12
0.4	0.9988	134.42	9.1E+10	0.998888	134.4252	8.5E+10
0.45	0.9978	137.59	1.4E+11	0.997876	137.5952	1.3E+11
0.5	0.9978	137.5	1.1E+11	0.997857	137.5048	1E+11
0.55	0.9978	137.41	8.6E+10	0.997869	137.4172	8E+10
0.6	0.998	143.71	2.4E+11	0.998032	143.7138	2.2E+11
0.65	0.9974	163.55	8.5E+12	0.997426	163.5525	7.9E+12
0.7	0.9927	191.47	9.2E+14	0.992714	191.4735	8.5E+14
0.75	0.9906	210.01	6.8E+15	0.990619	210.0109	6.3E+15
0.8	0.9871	155.19	4.4E+10	0.987183	155.1938	3.9E+10
0.85	0.9925	183.46	5.8E+11	0.99258	183.4688	5.3E+11
0.9	0.9947	191.05	7.1E+10	0.994792	191.053	6.4E+10

	FWO			Friedman		
α	**R^2**	**E_a**	**K_o**	**R^2**	**E_a**	**K_o**
0.05	0.9991	159.06	9.9E+14	0.996919	150.1296	2.7E+18
0.1	0.994	146.16	1.2E+13	0.988613	141.4099	1.4E+17
0.15	0.994	146.15	5.8E+12	0.998172	136.5432	3.8E+16
0.2	0.9981	147.52	9.5E+11	0.991866	120.41	1E+15
0.25	0.9929	155.5	3.2E+12	0.996053	142.1149	1E+17
0.3	0.9914	147.03	7.9E+11	0.99431	162.967	1.3E+19
0.35	0.9965	155.43	1.8E+12	0.998347	136.5717	2.2E+16
0.4	0.999	144.31	1.6E+11	0.99996	117.2269	3.3E+14
0.45	0.9981	147.56	2.4E+11	0.99385	144.6624	8.1E+16
0.5	0.9981	147.55	1.9E+11	0.99785	137.4417	1.5E+16
0.55	0.9981	147.53	1.6E+11	0.997325	148.23	1E+17
0.6	0.9982	153.92	3.9E+11	0.987541	177.4263	2.2E+19
0.65	0.9977	173.89	1.1E+13	0.98723	209.0069	4.8E+21
0.7	0.9934	202.04	9.4E+14	0.989419	220.3036	9.6E+21
0.75	0.9915	221	6.3E+15	0.991937	205.1704	6.9E+19
0.8	0.9888	166.83	7.8E+10	0.981322	146.5045	1.8E+14
0.85	0.9934	196.01	8.9E+11	0.994051	192.1974	3.6E+16
0.9	0.9954	205.04	1.2E+11	0.995477	194.162	1.6E+15

Table 6. Activation Energy(Ea(kJ/mol)) and Pre-exponential Factor, 4 Methods i.e. DAEM KAS, FWO and Friedman Straw with Ni-Ca_2SiO_4 Catalyst

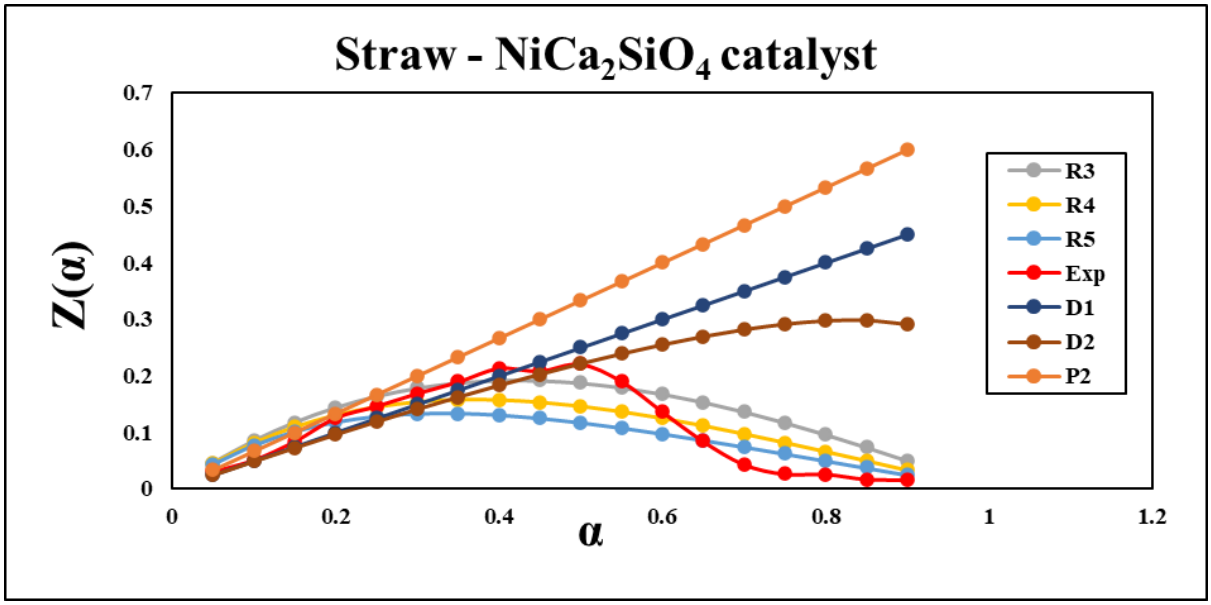

Figure 8. Master Plot for Straw with $NiCa_2SiO_4$ Catalyst

For Straw with $NiCa_2SiO_4$ Catalyst condition, it initially follows power law of nucleation with diffusion control mechanism until initial 15% but then suddenly changes to 4^{th} order chemical reaction for 20% to 25% and then shows 3rd order reaction for 30 to 35%, Diffusion-Controlled mechanism from 40% to 50% conversion and then order of reaction is continuously increased as conversion increases. The overall master plot demonstrated that pyrolysis of straw with $NiCa_2SiO_4$ catalyst is dominated by 3^{rd} order (R3) and 4^{th} order (R4) chemical reactions with diffusion-controlled mechanisms.

4.4.Sawdust Without Catalyst:

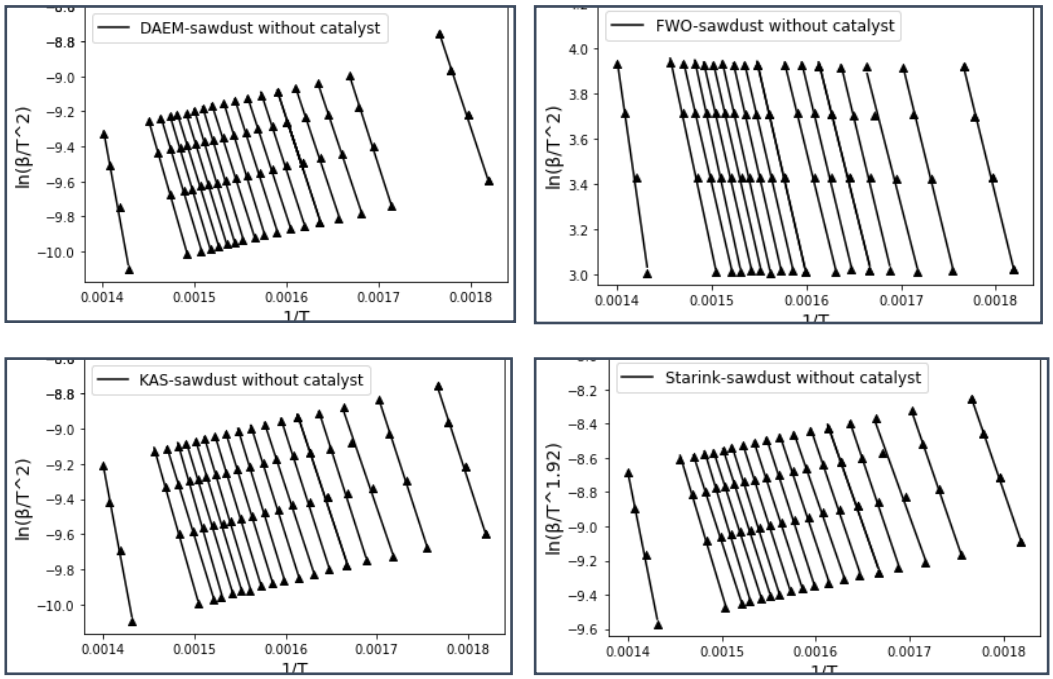

Figure 9.Arrhenius plot of Sawdust at different degrees from:
(a)DAEM ,(b)FWO, (c)KAS,(d)Starink methods

The Kinetics of sawdust biomass were determined by using 4 model free iso conversion Methods at a degree of freedom ranging from 0.05 to 0.9 showed in above figure. Arrhenius plot for Sawdust without catalyst at different degrees derived from 1) KAS, 2) DAEM, 3)FWO, 4)Starink methods, where arrows in each lines defines different heating rates varying from 20 to 50^{o}C/min. and each lines from Right to left Defines different degrees of freedom from 0.05 to 0.9.

Activation energy, overall correlation(R^2) and frequency defined from various methods at different degrees of freedom is defined below Table. Overall correlation (R^2) is above 0.9, which signifies that all the methods is suitable for modelling.

Straw activation energy without catalyst ranges from 134 to 283 KJ/mol. In the case of the FWO technique, the activation energy was 196-205 KJ/Mol at conversion stages 0.85-0.9. Furthermore, it exhibits a higher activation energy at the final stage of conversion, namely 283KJ/mol in the Friedman Method. As conversion increases, the pre-exponential factor gradually increases.

	FWO			Friedman		
α	**R^2**	**E_a**	**K_o**	**R^2**	**E_a**	**K_o**
0.05	0.9991	159.06	3.2E+11	0.9989	134.25	4.59E+14
0.1	0.994	146.16	2.1E+10	0.9917	127.86	5.28E+13
0.15	0.994	146.15	8.6E+09	0.9972	135.24	2.02E+14
0.2	0.9981	147.52	4E+09	0.9892	137.39	2.57E+14
0.25	0.9929	155.5	3.3E+09	0.999	131.22	5.78E+13
0.3	0.9925	147.03	3.8E+09	0.9998	134.09	8.35E+13
0.35	0.9965	155.43	2.9E+09	0.999	134.87	8.02E+13
0.4	0.999	144.31	2.2E+09	0.9982	153.71	2.76E+15
0.45	0.9981	147.56	4.2E+09	0.9994	143.31	2.88E+14
0.5	0.9981	147.55	1.6E+09	0.9991	141.07	1.61E+14
0.55	0.9981	147.53	2.2E+09	0.9994	145.93	3.53E+14
0.6	0.9982	153.92	3.1E+09	0.9847	141.83	1.46E+14
0.65	0.9977	173.89	2.5E+09	0.9971	140.36	9.94E+13
0.7	0.9934	202.04	4.9E+08	0.9966	155.91	1.52E+15
0.75	0.9915	221	7.7E+07	0.9998	139.99	6.05E+13
0.8	0.9888	166.83	5.7E+09	0.9984	121.53	1.31E+12
0.85	0.9934	196.01	1.2E+09	0.992	188.21	1.16E+17
0.9	0.9954	205.04	3.3E+12	0.9934	283.83	1.75E+23

	DAEM			KAS		
α	**R^2**	**E_a**	**K_o**	**R^2**	**E_a**	**K_o**
0.05	0.999	134.77	6.85E+11	0.999	134.77	6.44E+11
0.1	0.9989	134.02	1.92E+11	0.9989	134.02	1.79E+11
0.15	0.992	126.35	1.95E+10	0.992	126.35	1.83E+10
0.2	0.9981	136.34	9.98E+10	0.9981	136.34	9.43E+10
0.25	0.9981	130.67	2.12E+10	0.9981	130.67	1.99E+10
0.3	0.9989	134.92	3.62E+10	0.9989	134.92	3.4E+10
0.35	0.9996	130.83	1.17E+10	0.9996	130.83	1.09E+10
0.4	0.9993	136.05	2.55E+10	0.9993	136.05	2.38E+10
0.45	0.9994	140.05	4.28E+10	0.9994	140.05	4E+10
0.5	0.9999	138.26	2.37E+10	0.9999	138.26	2.2E+10
0.55	0.9999	140.93	3.19E+10	0.9999	140.93	2.96E+10
0.6	0.9996	140.33	2.3E+10	0.9996	140.33	2.14E+10
0.65	0.9983	140.9	2.15E+10	0.9983	140.9	2.02E+10
0.7	0.9996	140.19	1.57E+10	0.9996	140.19	1.46E+10
0.75	0.9992	147.76	5.4E+10	0.9992	147.76	5.07E+10
0.8	0.9998	137.8	6.85E+09	0.9998	137.8	6.33E+09
0.85	0.9988	148.43	3.74E+10	0.9988	148.43	3.5E+10
0.9	0.9961	224.24	6.63E+15	0.9961	224.24	6.44E+15

Table 7. Activation Energy(Ea(kJ/mol)) and Pre-exponential Factor, calculated from 4 Methods i.e. DAEM KAS, FWO and Friedman Sawdust without catalyst

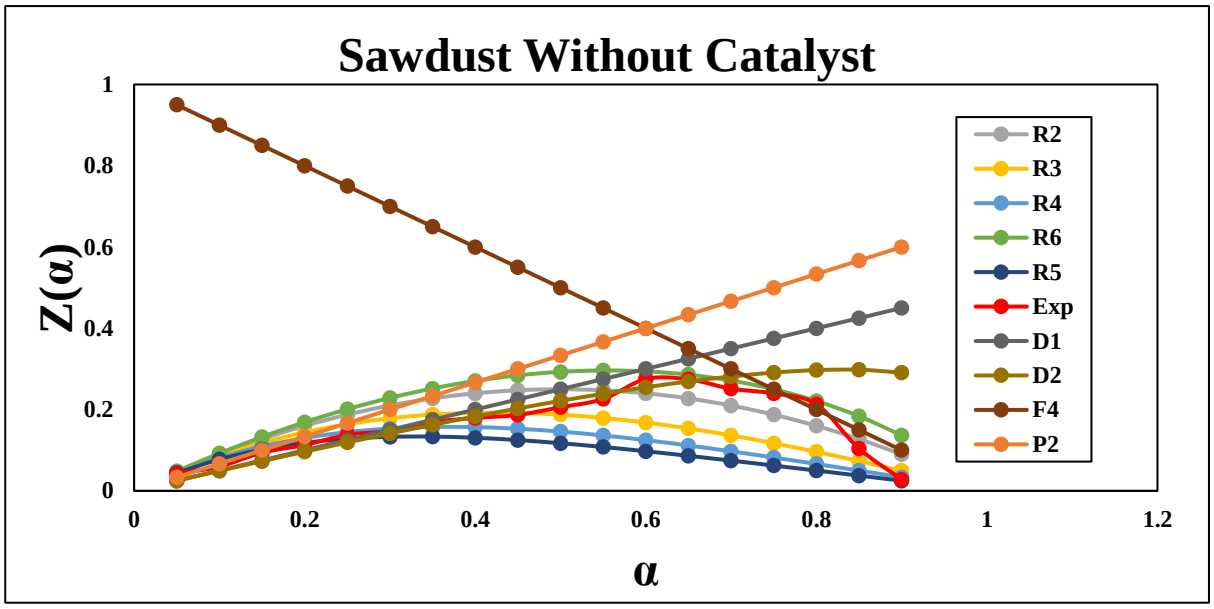

Figure 10. Master Plot for Sawdust Without Catalyst

This technique appears to be Diffusion-controlled Mechanism for Sawdust without Catalyst condition. Initially, the reaction followed a 5th order reaction, but as conversion increased, the reaction order decreased to a 3rd order reaction, and finally, it followed a one and a half order reaction. The experimental master plot is closer to the Jander equation in two and three dimensions. This diffusion-controlled process of sawdust with no catalyst is related with faster biomass breakdown. In summary, the master plot anticipated that Sawdust without a catalyst will undergo a one and a half order reaction (R6) using a diffusion-controlled mechanism.

4.5.Sawdust with $NiCaOSi_2O_4$:

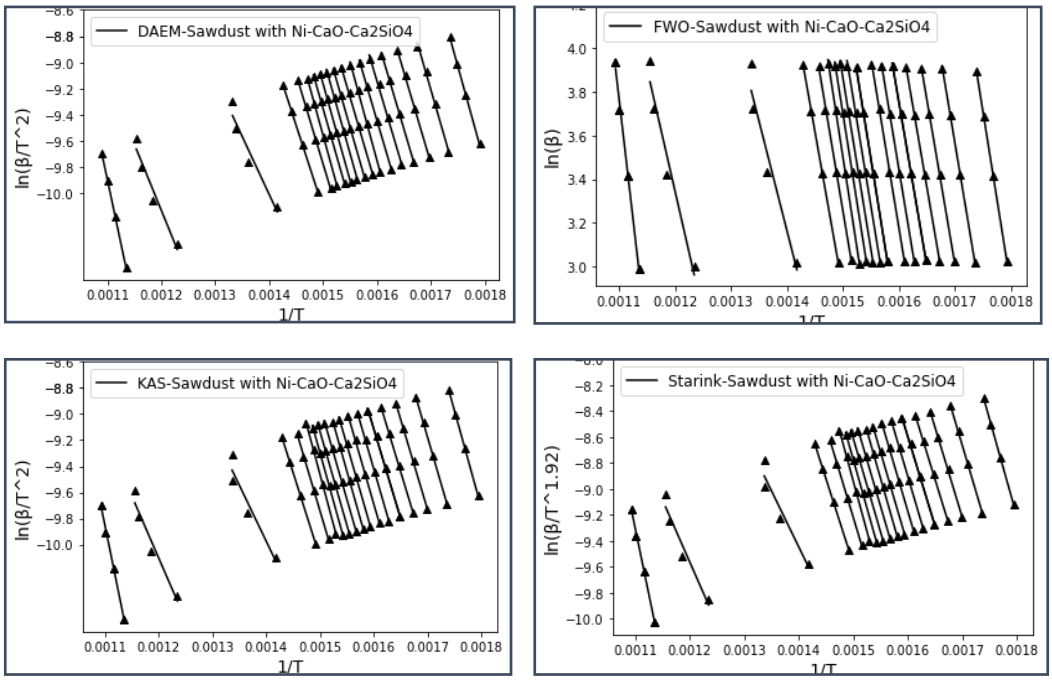

Figure 11.Arrhenius plot of sawdust with Ni-$CaOSi_2O_4$ catalyst at different degrees from: (a) DAEM, (b) FWO, (c) KAS (d)Starink methods

As indicated in the figure above, the kinetics of sawdust biomass were computed using four model free iso conversion techniques with degrees of freedom ranging from 0.05 to 0.9. Arrhenius plot for sawdust with $NiCaOSi_2O_4$ catalyst at different degrees created by 1) KAS, 2) DAEM, 3)FWO, and 4)Starink procedures, with arrows in each line denoting different heating rates ranging from 20 to 50^{o}C/min with each line moving from right to left. Defines a range of degrees of freedom from 0.05 to 0.9.

The table below defines the activation energy, overall correlation (R^2), and frequency calculated by various methodologies at various degrees of freedom. The total correlation (R^2) is more than 0.9, showing that all methods are suitable for modelling.

Sawdust activation energy with Ni-$CaOSi_2O_4$ catalyst ranges from 70 to 130 KJ/mol. And as the number of conversion steps increased, the activation energy decreased, but in the last stages, it scaled to 70-161 KJ/Mol. Which is less than without the catalyst condition, and the pre-exponential factor decreases gradually as conversion increases.

	DAEM			KAS		
α	**R^2**	**E_a**	**K_o**	**R^2**	**E_a**	**K_o**
0.05	0.9997	130.67	1.76E+11	0.9997	130.67	1.76E+11
0.1	0.9996	121.7	9.59E+09	0.9996	121.7	9.59E+09
0.15	0.9998	119.83	3.61E+09	0.9998	119.83	3.61E+09
0.2	0.9998	117.86	1.59E+09	0.9998	117.86	1.59E+09
0.25	0.999	118.63	1.28E+09	0.999	118.63	1.28E+09
0.3	0.9996	121.06	1.52E+09	0.9996	121.06	1.52E+09
0.35	0.9996	120.94	1.12E+09	0.9996	120.94	1.12E+09
0.4	0.9996	120.83	8.42E+08	0.9996	120.83	8.42E+08
0.45	0.9997	125.38	1.67E+09	0.9997	125.38	1.67E+09
0.5	0.9988	121.04	5.74E+08	0.9988	121.04	5.74E+08
0.55	0.9997	124.62	8.98E+08	0.9997	124.62	8.98E+08
0.6	0.9992	126.86	1.2E+09	0.9992	126.86	1.2E+09
0.65	0.9992	126.76	9.6E+08	0.9992	126.76	9.6E+08
0.7	0.9967	118.76	1.64E+08	0.9967	118.76	1.64E+08
0.75	0.9994	109.99	21876823	0.9994	109.99	21876823
0.8	0.9504	70.95	7.04E+08	0.9504	70.95	7.04E+08
0.85	0.9668	76.06	1.32E+08	0.9668	76.06	1.32E+08
0.9	0.9964	161.56	1.17E+12	0.9964	161.56	1.17E+12

	FWO			Friedman		
α	**R^2**	**E_a**	**K_o**	**R^2**	**E_a**	**K_o**
0.05	0.9997	133.16	1.2E+12	0.9994	121.09	6.11E+14
0.1	0.9996	124.94	3.5E+11	0.9997	116.73	1.28E+14
0.15	0.9998	123.37	4.2E+10	0.9998	116.06	9.27E+13
0.2	0.9999	121.65	1.9E+11	0.9963	117.19	9.52E+13
0.25	0.9992	122.53	4.5E+10	0.9987	124.3	3.19E+14
0.3	0.9996	124.96	7.4E+10	0.9995	124.85	2.99E+14
0.35	0.9996	124.96	2.6E+10	0.9996	120.93	1.14E+14
0.4	0.9996	124.95	5.3E+10	0.996	134.43	1.48E+15
0.45	0.9998	129.37	8.6E+10	0.9993	131.84	7.76E+14
0.5	0.999	125.33	4.9E+10	0.9968	122.42	9.16E+13
0.55	0.9997	128.84	6.5E+10	0.9915	142.82	4.77E+15
0.6	0.9994	131.03	4.8E+10	0.964	135.98	1.21E+15
0.65	0.9994	131.02	4.5E+10	0.9881	115.03	1.31E+13
0.7	0.9972	123.52	3.3E+10	0.9435	91.94	5.82E+12
0.75	0.9995	115.37	1.1E+11	0.9889	84.78	4.33E+11
0.8	0.9629	78.92	1.5E+10	0.8464	51.75	6.66E+17
0.85	0.9757	85.52	7.6E+10	0.9918	112.93	8.29E+14
0.9	0.997	167.75	6.8E+15	0.9951	250.61	1.12E+20

Table 8. Activation Energy(Ea(kJ/mol)) and Pre-exponential Factor, 4 Methods i.e. DAEM KAS, FWO and Friedman Sawdust with $NiCaOSi_2O_4$ Catalyst

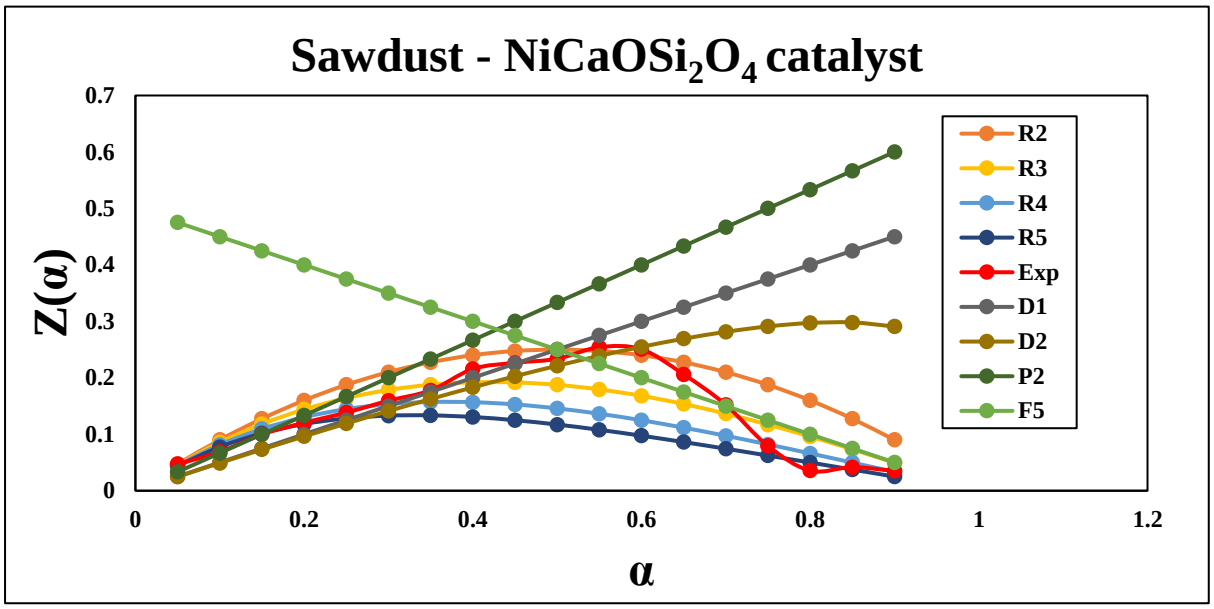

Figure 12. Master Plot for Sawdust - $NiCaOSi_2O_4$ catalyst

Sawdust with $NiCaOSi_2O_4$ catalyst follows power law of nucleation at conversions up to 15% and then starts following 4th order reaction, showing two-dimensional diffusion-controlled mechanism at 60% conversion. Order rection decreases to second order as conversion progresses, then climbs to fourth order in the last phases. Overall, this master plot anticipated a 4th order (R4) chemical reaction for sawdust with $NiCaOSi_2O_4$ catalyst using a diffusion-controlled nucleation mechanism.

4.6.Sawdust with Ni-Ca_2SiO_4 catalyst:

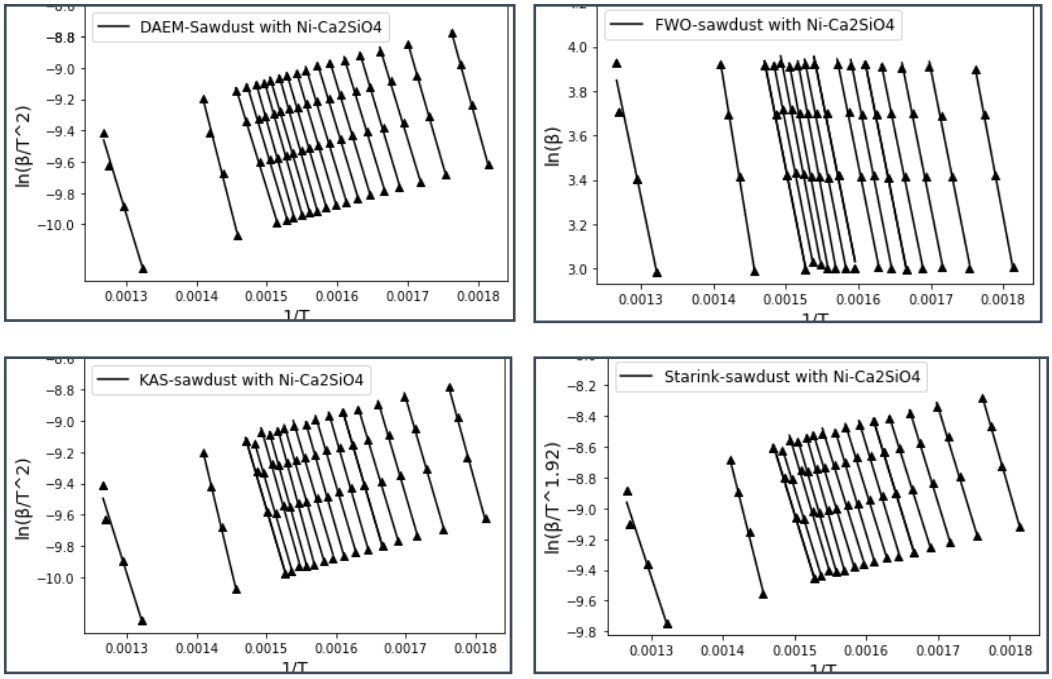

Figure 13.Arrhenius plot of sawdust with Ni-Ca_2SiO_4 catalyst at different degrees from (a) DAEM, (b)FWO, (c) KAS (d) Starink methods

The kinetics of sawdust biomass were determined using four model free iso conversion methods with degrees of freedom ranging from 0.05 to 0.9, as shown in the figure above. Arrhenius plot for sawdust with $NiCa_2SiO_4$ catalyst at various degrees derived from 1) KAS, 2) DAEM, 3)FWO, and 4)Starink methods, with arrows in each line defining different heating rates ranging from 20 to 50^0C/min. and each line from right to left defining different degrees of freedom ranging from 0.05 to 0.9.

The activation energy, overall correlation (R^2), and frequency defined by various approaches at various degrees of freedom are defined in the table below. The overall correlation (R^2) is more than 0.9, indicating that all of the approaches are adequate for modelling.

Sawdust activation energy with Ni-Ca_2SiO_4 catalyst ranges between 110 and 140 KJ/mol. And as the conversion steps progressed, it revealed variable activation energy that was steadily growing until it reached 112 KJ/Mol at the end. Which is less than without the catalyst condition, and the $NiCaOSi_2O_4$ Catalyst condition and the pre-exponential factor exhibited mixed behaviour. It steadily reduced in the DAEM, KAS, and FWO methods, but increased in the Friedman technique as conversion increased.

	DAEM			KAS		
α	**R^2**	**E_a**	**K_o**	**R^2**	**E_a**	**K_o**
0.05	0.9983	138.07	1.3E+12	0.9983	138.07	1.2E+12
0.1	0.9983	128.87	6.18E+10	0.9983	128.87	5.79E+10
0.15	0.9992	127.77	2.59E+10	0.9992	127.77	2.42E+10
0.2	0.9998	123.89	7.26E+09	0.9998	123.89	6.71E+09
0.25	0.9995	125.28	6.72E+09	0.9995	125.28	6.18E+09
0.3	0.9982	128.21	8.81E+09	0.9982	128.21	8.22E+09
0.35	0.9983	124.69	3.21E+09	0.9983	124.69	3E+09
0.4	0.9997	129.63	6.59E+09	0.9997	129.63	6.1E+09
0.45	0.9961	124.48	1.85E+09	0.9961	124.48	1.74E+09
0.5	0.9987	125.04	1.65E+09	0.9987	125.04	1.52E+09
0.55	0.9993	132.31	5.71E+09	0.9993	132.31	5.53E+09
0.6	0.9997	132.92	5.1E+09	0.9997	132.92	4.71E+09
0.65	0.9975	130.35	2.62E+09	0.9975	130.35	2.44E+09
0.7	0.9999	131.66	2.77E+09	0.9999	131.66	2.55E+09
0.75	0.9984	125.08	6.67E+08	0.9984	125.08	6.1E+08
0.8	0.9984	125.08	6.67E+08	0.9984	125.08	6.75E+08
0.85	0.9952	143.65	6.46E+09	0.9952	143.65	6.19E+09
0.9	0.9798	112.09	2578011	0.9798	112.09	2284338

	FWO			Friedman		
α	**R^2**	**E_a**	**K_o**	**R^2**	**E_a**	**K_o**
0.05	0.9985	140.08	2.1E+12	0.998	129.5	5.44E+15
0.1	0.9985	131.66	1.2E+11	0.9972	124.68	9.39E+14
0.15	0.9993	130.81	5.4E+10	0.9995	122.32	4.43E+14
0.2	0.9998	127.28	1.6E+10	0.9991	122.81	4.06E+14
0.25	0.9996	128.74	1.5E+10	0.9949	132.25	2.34E+15
0.3	0.9985	131.65	2E+10	0.9922	126.56	5.83E+14
0.35	0.9986	128.41	7.8E+09	0.999	129.95	9.47E+14
0.4	0.9997	133.2	1.5E+10	0.997	131.95	1.18E+15
0.45	0.9967	128.41	4.7E+09	0.9919	117.76	5.99E+13
0.5	0.9989	129.02	4.2E+09	0.9958	149.46	2.86E+16
0.55	0.9994	136.01	1.4E+10	0.9951	158.42	1.34E+17
0.6	0.9998	136.67	1.2E+10	0.9866	128.39	3.25E+14
0.65	0.9979	134.3	6.4E+09	0.9984	130.22	4.2E+14
0.7	0.9999	135.62	6.7E+09	0.986	120.37	5.25E+13
0.75	0.9987	129.44	1.8E+09	0.9792	97.14	4.98E+11
0.8	0.9987	129.44	2.2E+09	0.9801	113.75	7.72E+12
0.85	0.9959	147.57	1.5E+10	0.9861	161.5	3.65E+15
0.9	0.9836	118.77	1.1E+07	0.9644	102.51	7.24E+09

Table 9. Activation Energy(Ea(kJ/mol)) and Pre-exponential Factor, 4 Methods i.e. DAEM KAS, FWO and Friedman Sawdust with Ni-Ca_2SiO_4 Catalyst

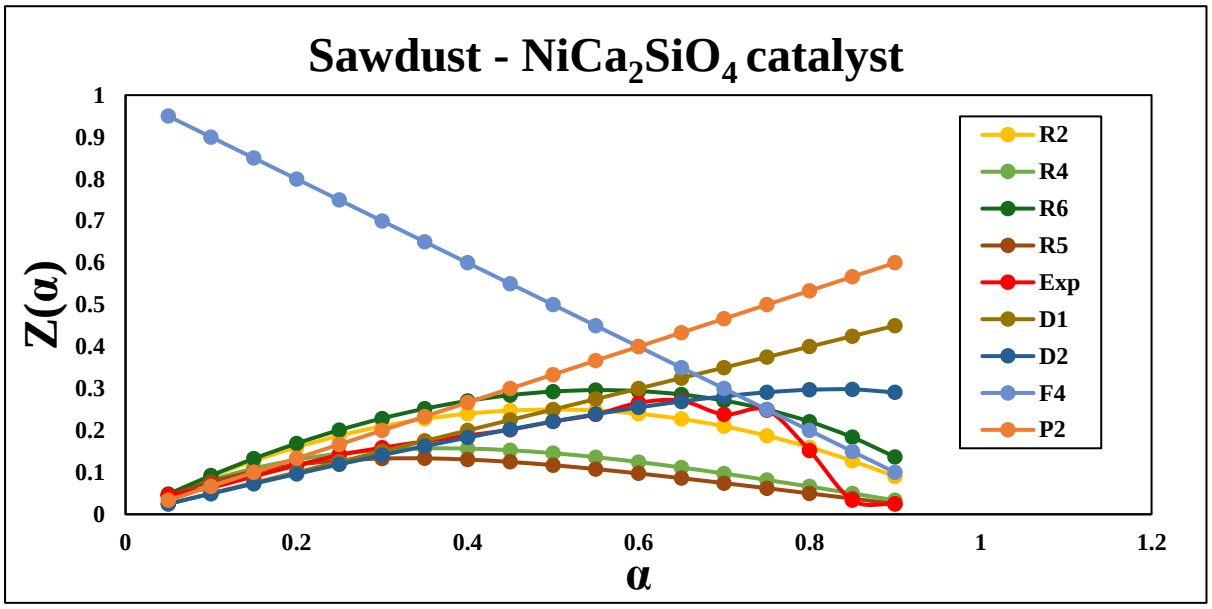

Figure 14. Master Plot for Sawdust with $NiCa_2SiO_4$ Catalyst

In sawdust with $NiCa_2SiO_4$ Catalyst, the process initially followed a fourth-order chemical reaction up to a point of 25% conversion before switching to a two-dimensional diffusion-controlled mechanism, which was projected to behave randomly at that point. And from 70% onward, a sudden change in order a chemical reaction of one and a half orders appears. This increase to second order was followed by a conversion that revealed a fifth order mechanism. In conclusion, Sawdust with $NiCa_2SiO_4$ Catalyst predicted R4 and R5 reaction mechanisms and had two diffusion-controlled reactions.

4.7.Cellulose Without Catalyst:

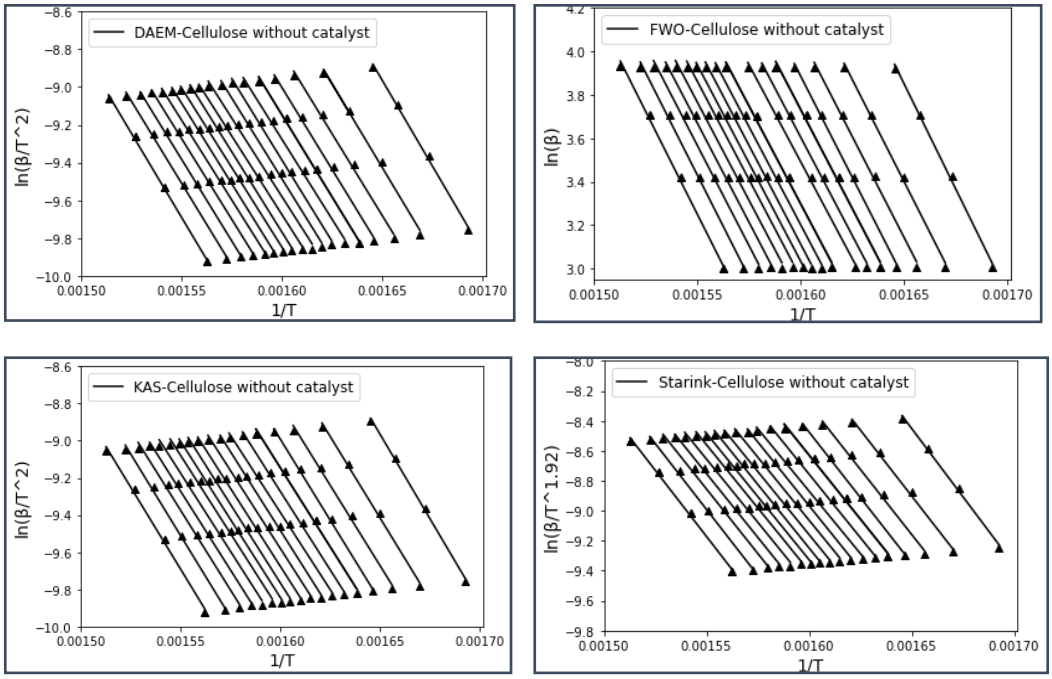

Figure 15.Arrhenius plot of Cellulose at different degrees from: (a) DAEM, (b)FWO, (c)KAS, (d) Starink methods

As shown in the above figure, the kinetics of cellulose biomass were calculated using four model free iso conversion methods with degrees of freedom ranging from 0.05 to 0.9. Arrhenius plot for cellulose without a catalyst at various degrees derived from 1) KAS, 2) DAEM, 3) FWO, and 4) Starink methods, where arrows in each line define different heating rates ranging from 20 to 50ºC/min and each line from right to left defines different degrees of freedom from 0.05 to 0.9.

Below is a table that defines activation energy, overall correlation (R^2), and frequency as they are defined using various methods and degrees of freedom. All of the methods are appropriate for modelling because the overall correlation (R^2) is above 0.9.

Without a catalyst, cellulose has an activation energy of 137–151 KJ/Mol. Additionally, it demonstrated a high activation energy at conversion stages 0.8 to 0.85, or 157 KJ/Mol in the case of the Friedman method. As conversion rates increased as conversion rises, activation energy decreased and the pre-exponential factor gradually shrank. It gradually decreased when using the DAEM, KAS, and FWO methods, but when using the Friedman method, it showed mixed results as conversion increased.

	DAEM			KAS		
α	**R^2**	**E_a**	**K_o**	**R^2**	**E_a**	**K_o**
0.05	0.9987	151.66	2.7E+13	0.9987	151.66	2.53E+13
0.1	0.998	148.06	8.18E+11	0.998	148.06	7.64E+11
0.15	0.9982	144.18	2.88E+11	0.9982	144.18	2.73E+11
0.2	0.9993	144.26	2.43E+11	0.9993	144.26	2.28E+11
0.25	0.9978	141.4	1.18E+11	0.9978	141.4	1.11E+11
0.3	0.9987	139.58	7.21E+10	0.9987	139.58	6.79E+10
0.35	0.9984	137.58	4.32E+10	0.9984	137.58	4.06E+10
0.4	0.9986	140.06	6.46E+10	0.9986	140.06	6.08E+10
0.45	0.9977	139.5	5.23E+10	0.9977	139.5	4.93E+10
0.5	0.9989	138.52	3.91E+10	0.9989	138.52	3.66E+10
0.55	0.9986	139.86	4.67E+10	0.9986	139.86	4.37E+10
0.6	0.9984	139.19	3.79E+10	0.9984	139.19	3.54E+10
0.65	0.9973	139.63	3.82E+10	0.9973	139.63	3.6E+10
0.7	0.9969	138.73	2.91E+10	0.9969	138.73	2.75E+10
0.75	0.9985	140.12	3.46E+10	0.9985	140.12	3.25E+10
0.8	0.9976	141.1	3.78E+10	0.9976	141.1	3.54E+10
0.85	0.9986	143.91	5.69E+10	0.9986	143.91	5.31E+10
0.9	0.9984	143.83	4.69E+10	0.9984	143.83	4.41E+10

	FWO			Friedman		
α	**R^2**	**E_a**	**K_o**	**R^2**	**E_a**	**K_o**
0.05	0.9989	153.64	4.1E+13	0.9961	144.11	4.16E+17
0.1	0.9983	150.35	1.3E+12	0.9971	135.7	6.64E+15
0.15	0.9984	146.74	5.1E+11	0.9996	138	1.25E+16
0.2	0.9994	146.87	4.3E+11	0.9953	135.25	7.76E+15
0.25	0.9981	144.2	2.2E+11	0.9929	125.87	1.22E+15
0.3	0.9989	142.52	1.4E+11	0.9996	123.75	8.1E+14
0.35	0.9987	140.65	8.7E+10	0.9973	145.25	6.22E+16
0.4	0.9988	143.05	1.3E+11	0.995	154.72	3.94E+17
0.45	0.998	142.54	1E+11	0.9816	132.62	4.36E+15
0.5	0.9991	141.64	7.9E+10	0.9955	140.72	2.07E+16
0.55	0.9988	142.95	9.3E+10	0.9894	143.18	3.43E+16
0.6	0.9986	142.35	7.7E+10	0.9789	138.04	1.24E+16
0.65	0.9977	142.79	7.8E+10	0.9631	138.39	1.13E+16
0.7	0.9973	141.97	6.1E+10	0.9996	141.85	1.75E+16
0.75	0.9987	143.33	7.1E+10	0.9966	153.7	1.53E+17
0.8	0.9979	144.29	7.7E+10	0.9866	157.28	2.41E+17
0.85	0.9988	147.01	1.1E+11	0.9993	156.28	1.32E+17
0.9	0.9986	147	9.4E+10	0.9794	143.34	7.93E+15

Table 10. Activation Energy(Ea(kJ/mol)) and Pre-exponential Factor, 4 Methods i.e. DAEM KAS, FWO and Friedman Cellulose without catalyst

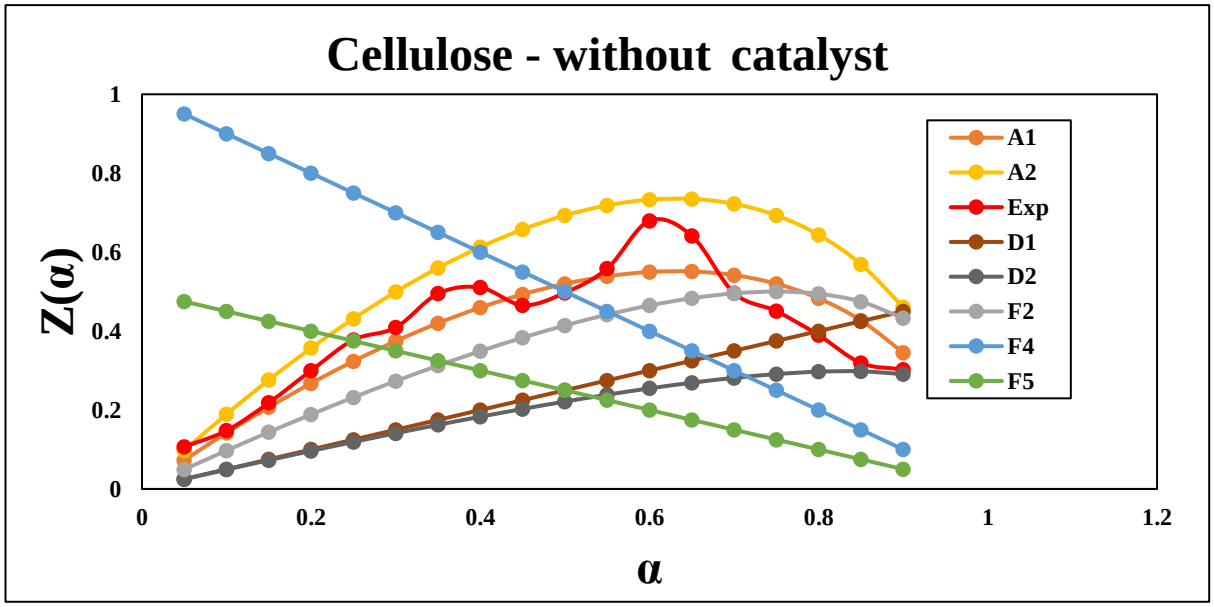

Figure 16. Master Plot for Cellulose without Catalyst

The overall process in Cellulose Without Catalyst followed the Avarami-Erofeev Sigmoidal Rate Equation and the Random Nucleation Mechanism. Additionally, it appears to be a two-dimensional diffusion-controlled mechanism at the point of conversion. Avarami-erofeev sigmoidal rate equation with random nucleation and diffusion-controlled mechanisms is foreseen in the overall master plot.

4.8.Cellulose with Ni-CaOSi_2O_4 catalyst:

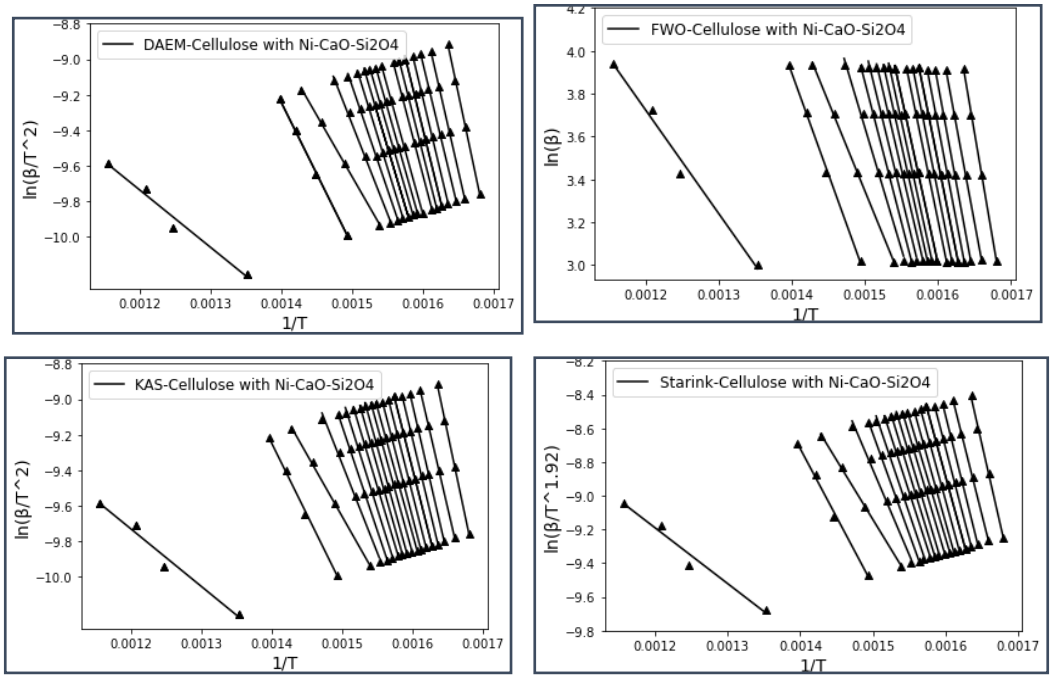

Figure 17.Arrhenius plot of Cellulose with Ni-CaO-Si_2O_4 catalyst at different degrees from: (a) DAEM, (b) FWO, (c) KAS (d)Starink methods

The cellulose biomass kinetics are shown in the figure above. Arrhenius plot for cellulose with $NiCaOSi_2O_4$ catalyst at various degrees derived from 1) KAS, 2) DAEM, 3) FWO, and 4) Starink methods; each line from right to left defines a different degree of freedom ranging from 0.05 to 0.9.

The table below defines activation energy, overall correlation (R^2), and frequency as determined by various techniques at various degrees of freedom. Overall correlation (R^2) is greater than 0.9, indicating that all approaches are appropriate for modelling.

With a $NiCaOSi_2O_4$ catalyst, cellulose has an activation energy that ranges from 159 to 83 KJ/mol. And as the number of conversion stages grew, the activation energy fluctuated and fell steadily until it reached 70-25 KJ/Mol at the very end. which is less than the condition without the catalyst. As conversion rises, the pre-exponential factor gradually declines.

	DAEM			KAS		
α	**R^2**	**E_a**	**K_o**	**R^2**	**E_a**	**K_o**
0.05	0.9983	159.27	1.02E+13	0.9983	159.27	1.02E+13
0.1	0.9994	145.94	4.32E+11	0.9994	145.94	4.32E+11
0.15	0.9995	146.52	3.68E+11	0.9995	146.52	3.68E+11
0.2	0.9998	140.18	8.54E+10	0.9998	140.18	8.54E+10
0.25	0.9998	131.5	1.27E+10	0.9998	131.5	1.27E+10
0.3	0.9999	132.02	1.21E+10	0.9999	132.02	1.21E+10
0.35	0.9997	129.27	6.14E+09	0.9997	129.27	6.14E+09
0.4	0.9995	120.3	9.25E+08	0.9995	120.3	9.25E+08
0.45	0.9995	121.67	1.09E+09	0.9995	121.67	1.09E+09
0.5	0.9988	120.87	8.25E+08	0.9988	120.87	8.25E+08
0.55	0.9995	117.45	3.79E+08	0.9995	117.45	3.79E+08
0.6	0.9993	111.07	97145602	0.9993	111.07	97145602
0.65	0.9975	106.35	33896606	0.9975	106.35	33896606
0.7	0.9995	98.81	6854225	0.9995	98.81	6854225
0.75	0.9955	84.18	334802.1	0.9955	84.18	334802.1
0.8	0.9991	57.96	1515.474	0.9991	57.96	1515.474
0.85	0.9976	67.15	6187.091	0.9976	67.15	6187.091
0.9	0.9838	25.87	0.753123	0.9838	25.87	0.753123

	FWO			Friedman		
α	**R^2**	**E_a**	**K_o**	**R^2**	**E_a**	**K_o**
0.05	0.9985	160.93	1.4E+13	0.9991	127.35	3.12E+13
0.1	0.9994	148.39	7.4E+11	0.7483	59.22	22445027
0.15	0.9996	149.03	6.3E+11	0.9997	127.39	3.24E+13
0.2	0.9998	143.06	1.6E+11	0.9942	97.36	7.62E+10
0.25	0.9998	134.87	2.7E+10	0.9975	110.85	1.11E+12
0.3	0.9999	135.42	2.6E+10	0.99	123.13	1.26E+13
0.35	0.9997	132.85	1.4E+10	0.9733	76.56	1.07E+09
0.4	0.9996	124.37	2.4E+09	0.9641	84.27	5.14E+09
0.45	0.9996	125.72	2.8E+09	0.9584	123.24	1.05E+13
0.5	0.999	125.02	2.2E+09	0.9924	102.31	1.51E+11
0.55	0.9996	121.81	1.1E+09	0.9763	73.98	4.9E+08
0.6	0.9994	115.8	3.1E+08	0.9618	67.35	1.04E+08
0.65	0.998	111.37	1.2E+08	0.9156	56.29	9245159
0.7	0.9995	104.26	2.7E+07	0.8405	29.82	28381.45
0.75	0.9966	90.47	1817383	-0.3035	-4.68	-4.73111
0.8	0.9994	65.75	15640.1	0.4964	13.79	220.1996
0.85	0.9982	74.76	51695.3	0.9813	83.34	98044351
0.9	0.9922	37.17	27.1816	0.6953	6.93	3.567781

Table 11. Activation Energy(Ea(kJ/mol)) and Pre-exponential Factor, 4 Methods i.e. DAEM KAS, FWO and Friedman Cellulose with $NiCaOSi_2O_4$ Catalyst

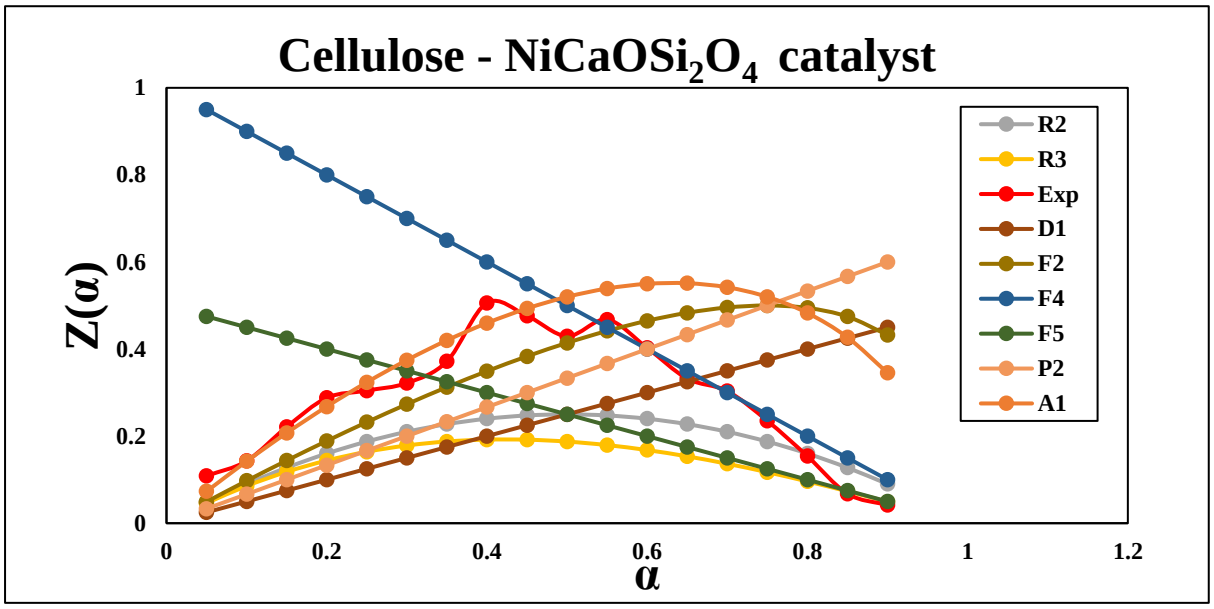

Figure 18. Master Plot for Cellulose with $NiCaOSi_2O_4$ Catalyst

Avarami-Erofeev sigmoidal rate equation and random nucleation mechanism were used in the overall conversion of cellulose with $NiCaOSi_2O_4$ catalyst, as well as for the third order reaction mechanism. Overall, the Avarami-Erofeev sigmoidal rate equation (A1) chemical reaction was anticipated by the Master Plot for Cellulose with $NiCaOSi_2O_4$ Catalyst; however, at the final stage, it appears to be a 3rd order (R3) chemical reaction with a diffusion-controlled and random nucleation mechanism. This demonstrates how using a $NiCaOSi_2O_4$ catalyst changed the way reactions happened, which is useful for producing specific types of biofuels.

4.9.Cellulose with Ni-Ca_2SiO_4 catalyst:

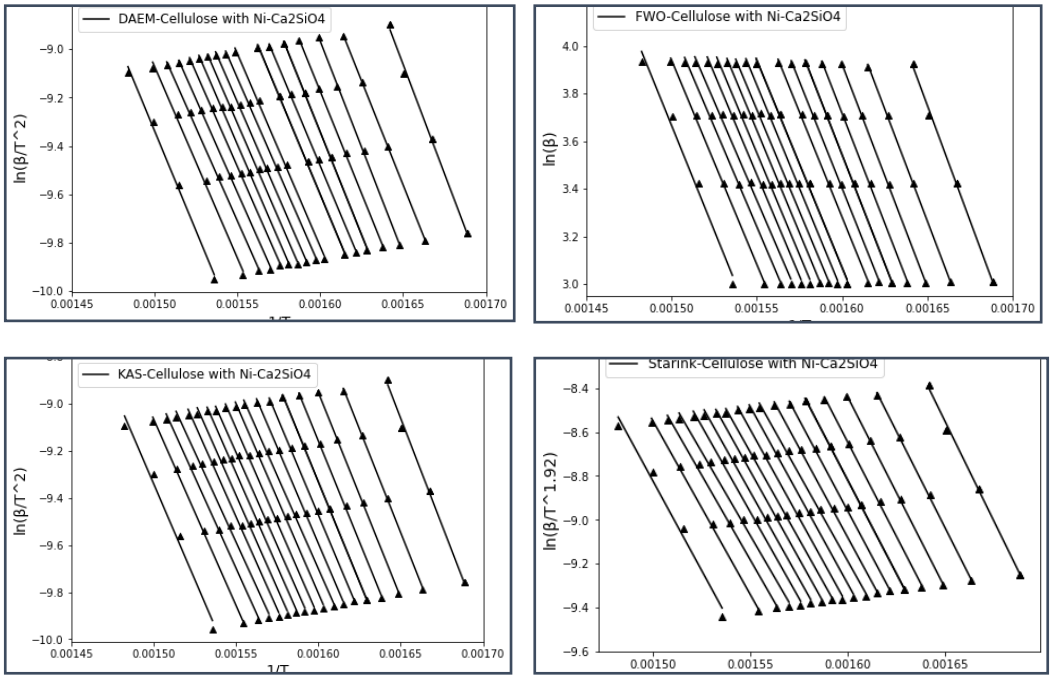

Figure 19.Arrhenius plot of Cellulose with Ni-Ca_2SiO_4 catalyst at different degrees from (a) DAEM, (b)FWO, (c) KAS (d) Starink methods

Utilising four model free iso conversion methods with degrees of freedom ranging from 0.05 to 0.9, the kinetics of cellulose biomass were determined. Arrhenius plot for cellulose with $NiCa_2SiO_4$ catalyst at various degrees derived from 1) KAS, 2) DAEM, 3) FWO, and 4) Starink methods; each line from right to left defines a different degree of freedom ranging from 0.05 to 0.9.

The table below defines activation energy, overall correlation (R^2), and frequency as determined by various techniques at various degrees of freedom. The overall correlation (R^2) is more than 0.9, indicating that all approaches are appropriate for modelling.

The Activation energy Cellulose with Ni-Ca_2SiO_4 catalyst has a KJ/mol range of 125–150. And as the number of conversion stages grew, the activation energy fluctuated and kept rising until the final conversion stages, when it dropped to 133 KJ/Mol. which is greater than NiCaOSi2O4 but less than the condition without the catalyst Pre-exponential factor and catalyst condition displayed inconsistent behaviour. It steadily dropped while using the DAEM, KAS, and FWO methods, but when using the Friedman technique, it had mixed behaviour as conversion increased.

.

	DAEM			KAS		
α	**R^2**	**E_a**	**K_o**	**R^2**	**E_a**	**K_o**
0.05	0.9976	149.94	1.73E+12	0.9976	149.94	1.6E+12
0.1	0.9999	147.92	7.02E+11	0.9999	147.92	6.55E+11
0.15	0.9998	144.58	2.69E+11	0.9998	144.58	2.51E+11
0.2	0.9997	142.33	1.4E+11	0.9997	142.33	1.31E+11
0.25	0.9998	140.24	7.73E+10	0.9998	140.24	7.19E+10
0.3	0.9995	138.83	5.07E+10	0.9995	138.83	4.74E+10
0.35	0.9994	135.15	2.15E+10	0.9994	135.15	2.01E+10
0.4	0.9994	129.86	6.74E+09	0.9994	129.86	6.25E+09
0.45	0.9991	132.67	1.07E+10	0.9991	132.67	9.94E+09
0.5	0.9993	131.55	7.74E+09	0.9993	131.55	7.2E+09
0.55	0.9995	130.43	5.62E+09	0.9995	130.43	5.21E+09
0.6	0.9992	130.76	5.5E+09	0.9992	130.76	5.11E+09
0.65	0.9984	129.82	4.17E+09	0.9984	129.82	3.89E+09
0.7	0.9984	128.49	2.95E+09	0.9984	128.49	2.75E+09
0.75	0.9985	125.5	1.48E+09	0.9985	125.5	1.37E+09
0.8	0.9986	126.92	1.75E+09	0.9986	126.92	1.62E+09
0.85	0.9994	129.47	2.46E+09	0.9994	129.47	2.27E+09
0.9	0.9929	133.01	3.65E+09	0.9929	133.01	3.47E+09

	FWO			Friedman		
α	**R^2**	**E_a**	**K_o**	**R^2**	**E_a**	**K_o**
0.05	0.9979	152.02	2.7E+12	0.9964	146.45	5.73E+16
0.1	0.9999	150.25	1.2E+12	0.9983	138.99	1.06E+16
0.15	0.9999	147.17	4.8E+11	0.9982	133.75	4.17E+15
0.2	0.9997	145.09	2.6E+11	0.9978	131.02	2.47E+15
0.25	0.9998	143.16	1.5E+11	0.9978	129.66	1.91E+15
0.3	0.9996	141.87	1E+11	0.9948	118.82	2.23E+14
0.35	0.9995	138.41	4.5E+10	0.9967	96.77	2.59E+12
0.4	0.9995	133.43	1.5E+10	0.998	123.6	5.66E+14
0.45	0.9992	136.14	2.4E+10	0.996	141.6	1.9E+16
0.5	0.9994	135.11	1.7E+10	0.9995	120.42	2.58E+14
0.55	0.9995	134.09	1.3E+10	0.9968	127.78	1.08E+15
0.6	0.9993	134.43	1.3E+10	0.9845	129.44	1.43E+15
0.65	0.9986	133.57	9.9E+09	0.9859	118.5	1.5E+14
0.7	0.9986	132.34	7.2E+09	0.9987	108.35	1.72E+13
0.75	0.9987	129.55	3.8E+09	0.9938	119.78	1.32E+14
0.8	0.9988	130.94	4.4E+09	0.9983	142.33	7.96E+15
0.85	0.9995	133.42	6E+09	0.997	146.93	1.04E+16
0.9	0.994	136.91	8.9E+09	0.9311	146.84	5.56E+15

Table 12. Activation Energy(Ea(kJ/mol)) and Pre-exponential Factor, 4 Methods i.e. DAEM KAS, FWO and Friedman Cellulose with Ni-Ca_2SiO_4 Catalyst

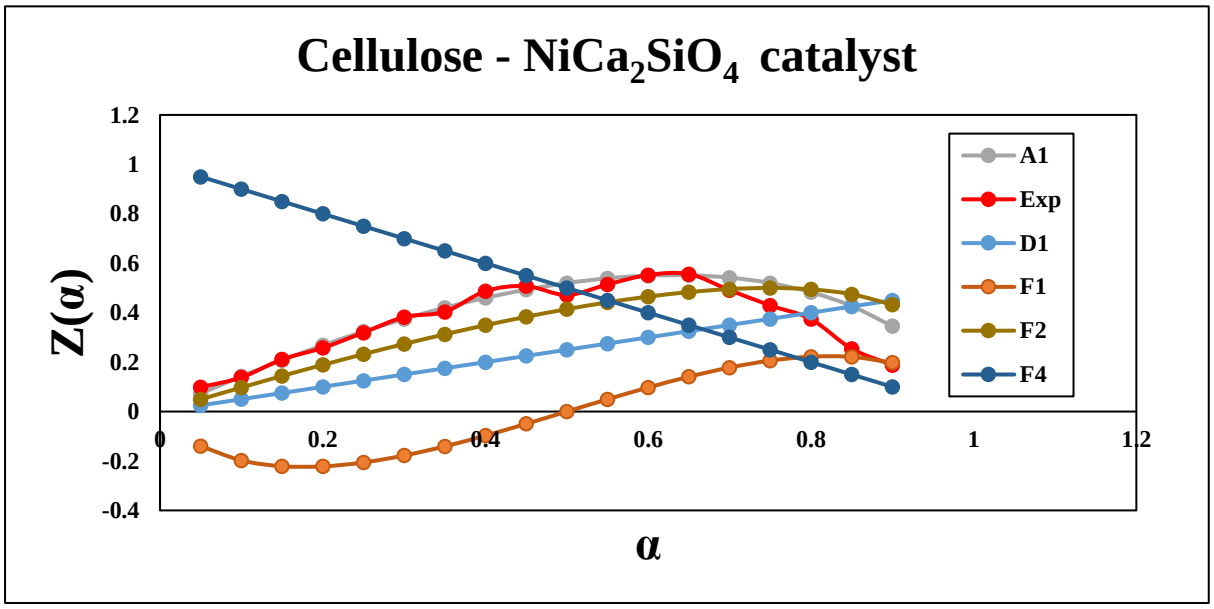

Figure 20. Master Plot for Cellulose with $NiCa_2SiO_4$ Catalyst

In the case of cellulose with $NiCa_2SiO_4$ catalyst, the process followed the Avarami-erofeev sigmoidal rate equation up to 65% conversion and then demonstrated random nucleation at 50% conversion, diffusion control of the reaction at 75% to 80% conversion, and Prout-Tomkins random nucleation at the final conversion. The Avarami-erofeev sigmoidal rate equation is shown to have strong control in the prediction produced by the master plot, which was made by the model motorway. These plots are therefore more significant.

4.10.Comparative Studies of Kinetic Parameters:

The graph below depicts how activation energy varies :	The graph below depicts how Pre-exponetial Factor varies :
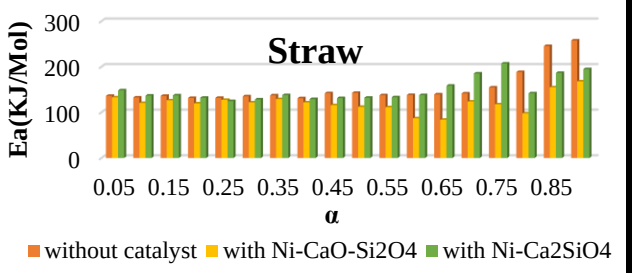	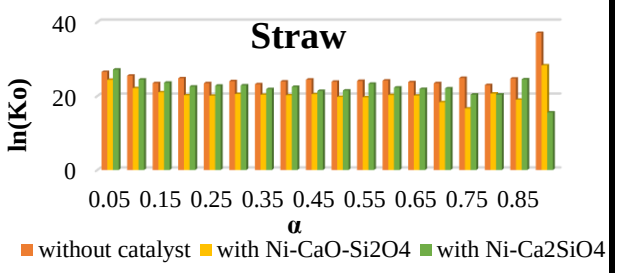
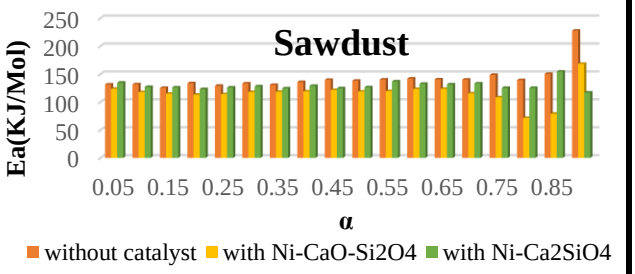	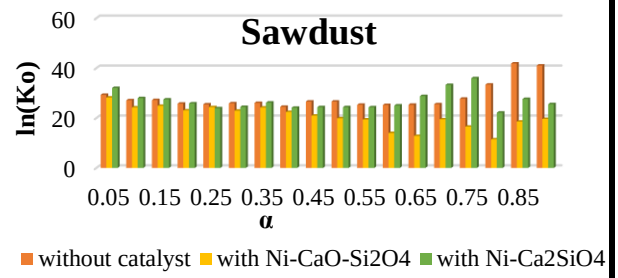
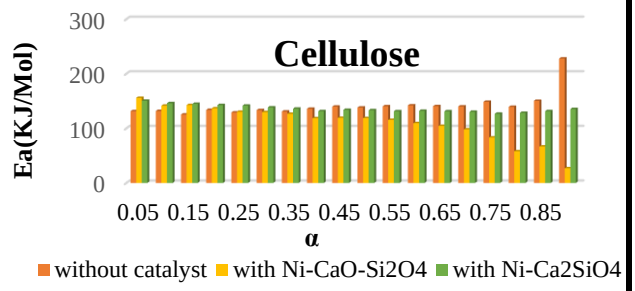	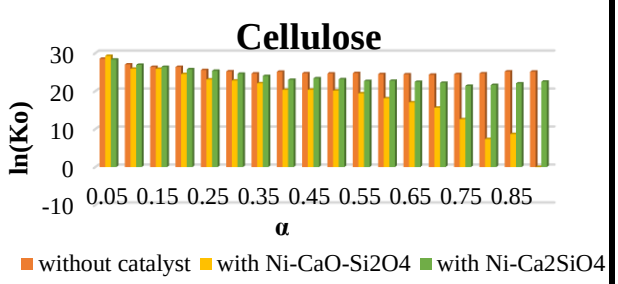

Figure 21. Comparative study of kinetic Parameters

The results indicate that the use of catalysts can significantly lower the activation energy required for the conversion of these biomass materials, as evidenced by the lower ranges of activation energy with catalysts compared to without catalysts. Specifically, the Ni-$CaOSi_2O_4$ catalyst consistently resulted in the lowest activation energies across all three materials.

In terms of pre-exponential factors, the data show that the use of catalysts can also significantly affect the frequency of molecular collisions. However, the trends observed for pre-exponential factors were less consistent than those for activation energies.

Overall, the results suggest that the use of Ni-$CaOSi_2O_4$ catalyst may be a promising strategy for reducing the energy required for the conversion of biomass materials, which could have important implications for the development of sustainable energy sources

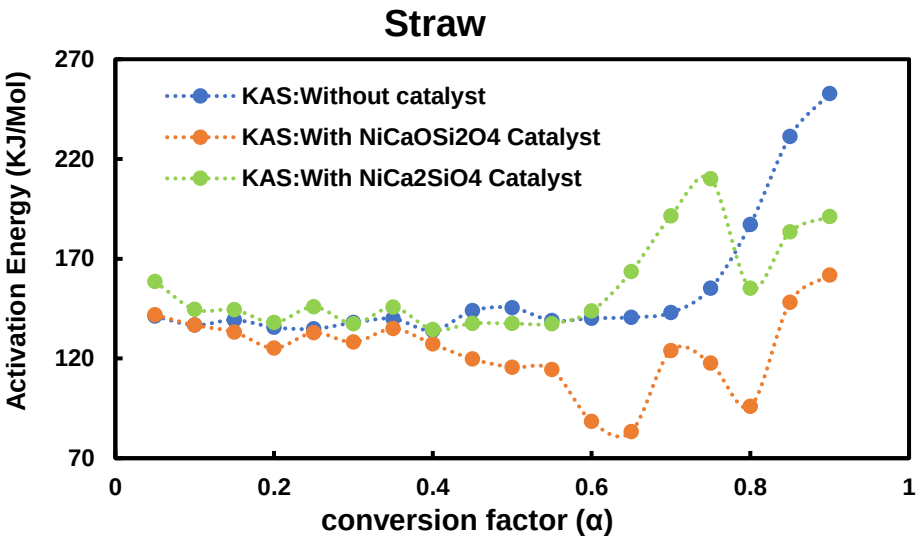

Figure 22.1
Change of Activation energy of Straw with KAS method under three catalytic conditions

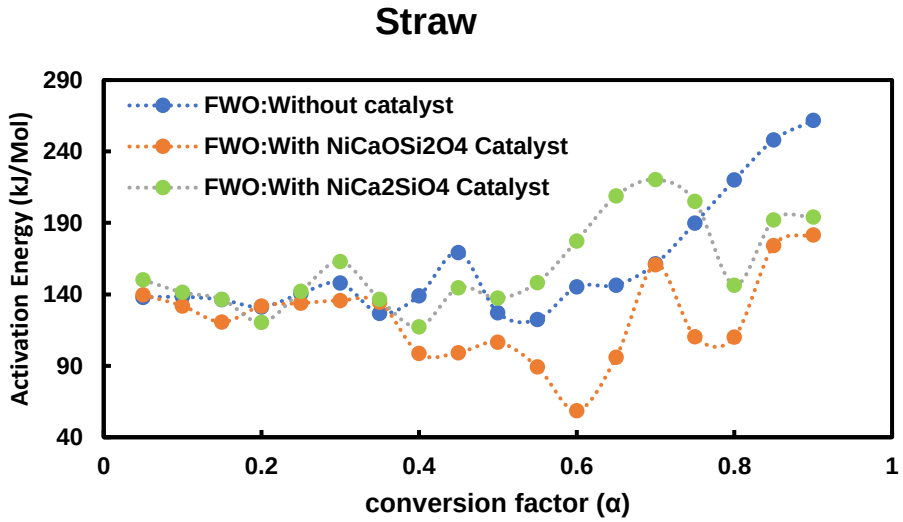

Figure 22.2
Change of Activation energy of Straw with FWO method under three catalytic conditions

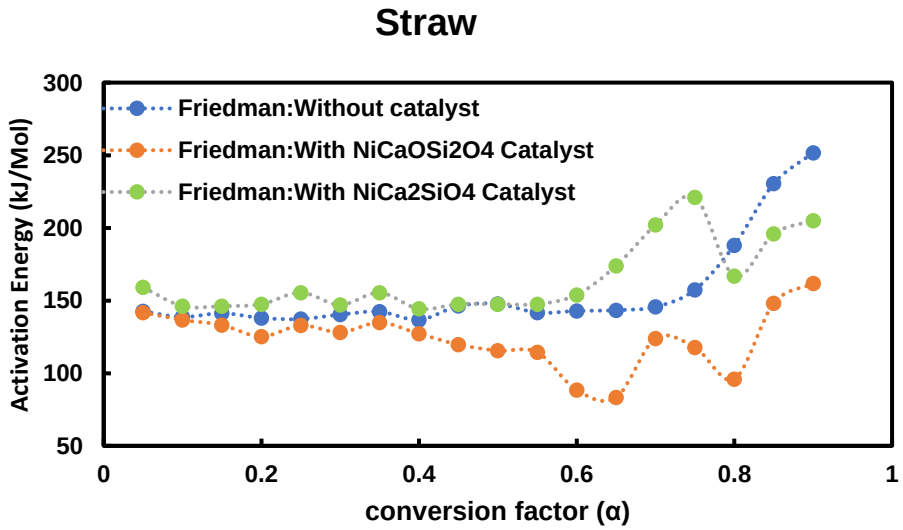

Figure 22.3
Change of Activation energy of Straw with Friedman method under three catalytic conditions

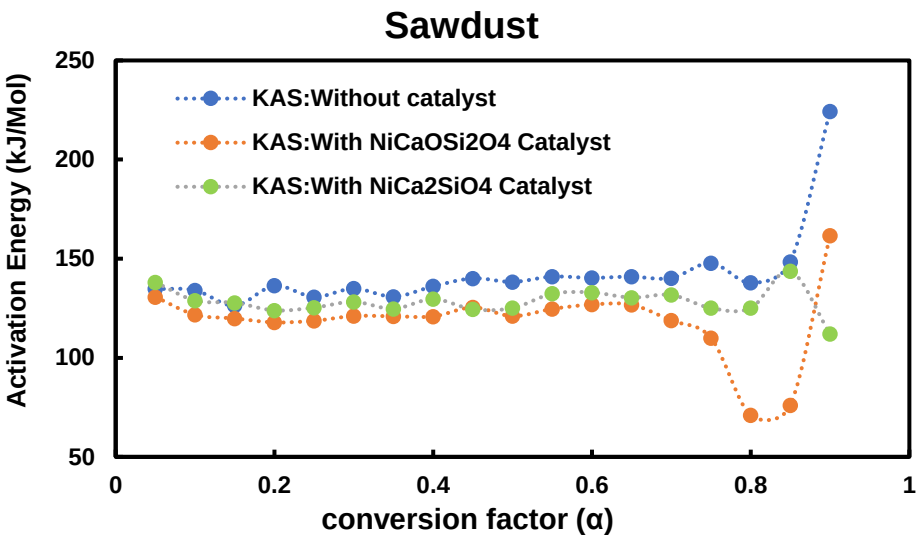

Figure 23.1
Change of Activation energy of Sawdust with KAS method under three catalytic conditions

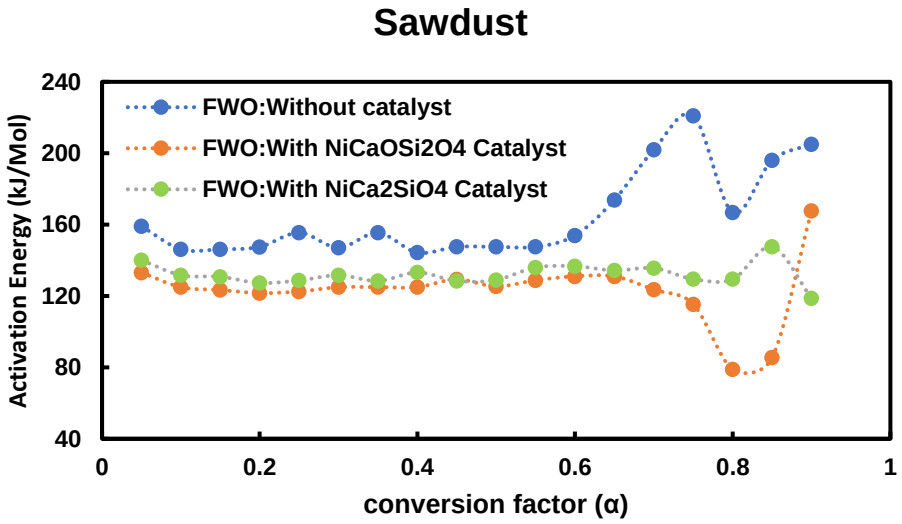

Figure 23.2
Change of Activation energy of Sawdust with FWO method under three catalytic conditions

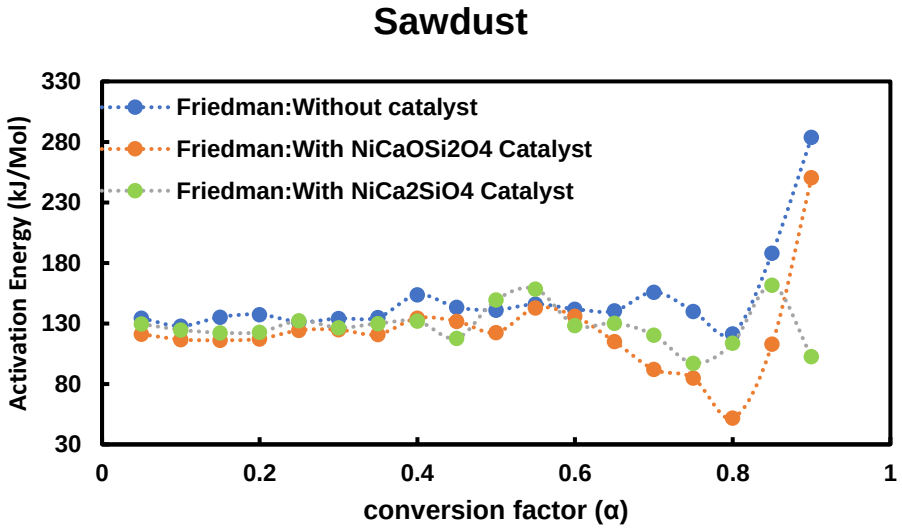

Figure 23.3
Change of Activation energy of Sawdust with Friedman method under three catalytic conditions

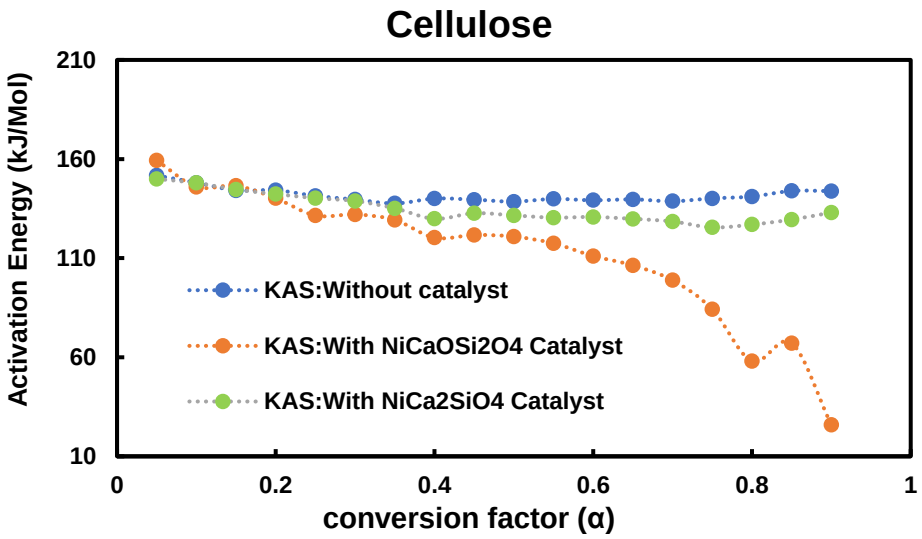

Figure 24.1
Change of Activation energy of Cellulose with KAS method under three catalytic conditions

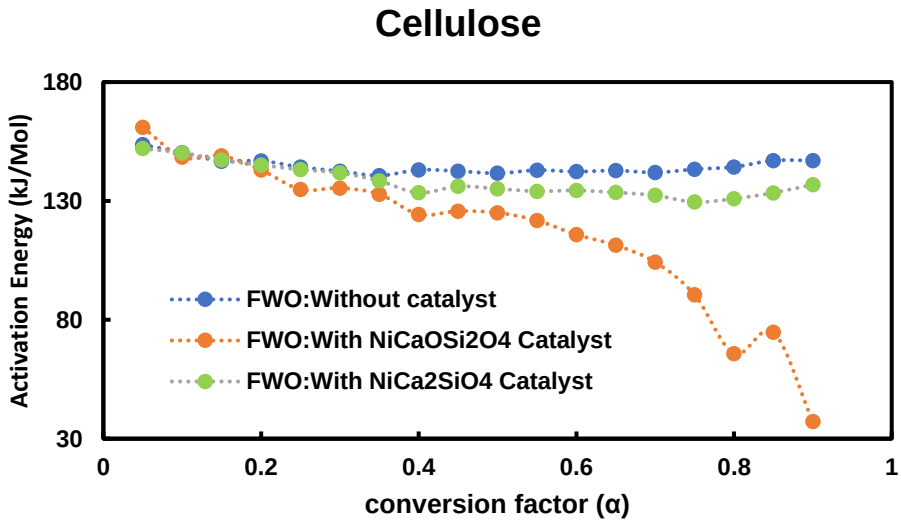

Figure 24.2
Change of Activation energy of Cellulose with FWO method under three catalytic conditions

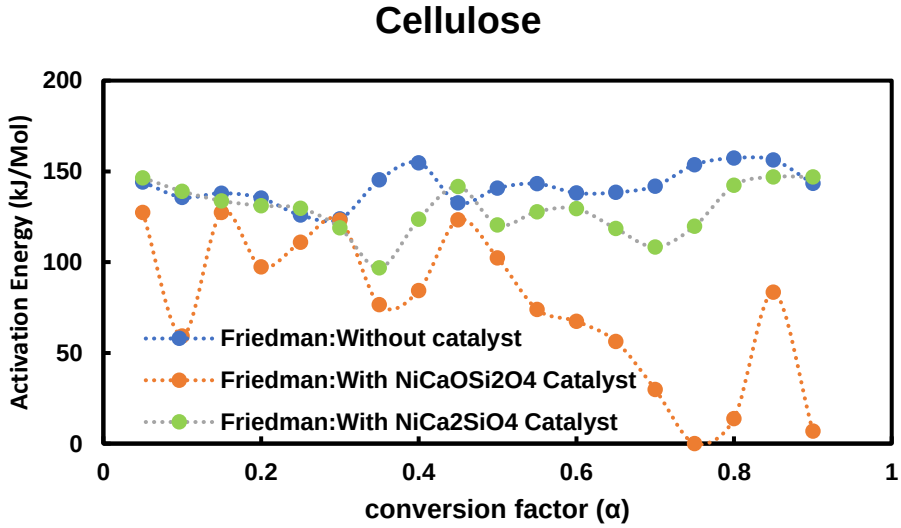

Figure 24.3
Change of Activation energy of Cellulose with Friedman method under three catalytic conditions

Figure 22.1 represents the Kissingers Aakhira-Sunose (KAS) method of kinetic analysis for straw under three different conditions: without catalyst, with $NiCaOSi_2O_4$ catalyst, and with $NiCa_2SiO_4$ catalyst, with α as the conversion factor.
Looking at the graph, we can see that the activation energy for the straw without catalyst ranges from 133.95 to 252.79, while the activation energy for the straw with catalyst ranges from 134.43 to 210.01. This suggests that the presence of the catalyst can lower the activation energy required for the reaction to occur.
Comparing the two catalysts used, we can see that in most cases, the $NiCa_2SiO_4$ catalyst has a lower activation energy compared to $NiCaOSi_2O_4$ catalyst, indicating that it is a more effective catalyst for this particular reaction.
Additionally, we can see that there is a significant increase in activation energy at α=0.75 for all three conditions, which may be attributed to changes in the reaction mechanism or other factors.
Overall, this data provides insights into the effect of catalysts on the kinetics of the reaction and can be useful in the development of more efficient catalytic systems for the conversion of straw.

Figure 22.2 consists of the conversion factor α and the activation energy (in kJ/mol) of straw under three conditions (without catalyst, with $NiCaOSi_2O_4$ catalyst, and with $NiCa_2SiO_4$ catalyst) using the FWO kinetic analysis method.
Looking at the data, it appears that the activation energy of straw generally decreases with increasing α for all three conditions. This trend is most noticeable for the without catalyst condition, where the activation energy drops from 137.92 kJ/mol at α = 0.05 to 220.07 kJ/mol at α = 0.8 before decreasing again to 248.12 kJ/mol at α = 0.85 and 261.70 kJ/mol at α = 0.9.
For the two catalyst conditions, the activation energy generally fluctuates around a certain range, with some values higher or lower than others. However, in general, the $NiCa_2SiO_4$ catalyst appears to have a lower activation energy than the $NiCaOSi_2O_4$ catalyst for most values of α.

The Figure 22.3 represents the results of the Friedman method of kinetic analysis for the conversion of straw under three different conditions, without catalyst, with $NiCaOSi_2O_4$ catalyst, and with $NiCa_2SiO_4$ catalyst, with varying values of α.
The conversion of straw generally increases with increasing values of α, for all three conditions.
The use of catalysts generally results in higher conversion of straw, compared to the condition without catalyst, for most values of α. The highest conversion is observed in the presence of $NiCa_2SiO_4$ catalyst.
The effect of catalysts on conversion of straw is more pronounced at lower values of α, while the effect diminishes at higher values of α.
The rate of increase in conversion with increasing values of α is generally higher for the condition without catalyst compared to the conditions with catalysts.
Overall, the data suggests that the use of $NiCa_2SiO_4$ catalyst is the most effective for increasing the conversion of straw under these conditions. However, further studies are needed to optimize the conditions and determine the feasibility of scaling up the process for industrial applications.

Figure 23.1 represent sawdust with three conditions using the KAS method of kinetic analysis, The activation energy for the decomposition of sawdust decreases with the use of catalysts $NiCaOSi_2O_4$ and $NiCa_2SiO_4$ compared to the case without a catalyst. The decomposition of sawdust is faster with the use of catalyst $NiCa_2SiO_4$ compared to the case with $NiCaOSi_2O_4$ or without a catalyst. The reaction rate increases with the increase of the conversion factor α until it reaches a maximum value, after which it decreases again. At higher conversion factors, there

is a significant increase in the reaction rate with the use of catalyst $NiCa_2SiO_4$ compared to the case without a catalyst or with $NiCaOSi_2O_4$.
Overall, the use of the KAS method of kinetic analysis provides valuable information about the reaction kinetics of sawdust decomposition and the effect of catalysts on the reaction rate and activation energy.

Figure 23.2 represents the results of the kinetic analysis of sawdust under three different conditions using the FWO method.
it is observed that the reaction rate decreases as the conversion factor α increases. This can be seen across all three conditions and with all three catalysts. This indicates that as the reaction progresses, the rate of conversion decreases. It can also be observed that the addition of the $NiCa_2SiO_4$ catalyst generally leads to higher reaction rates compared to the $NiCaOSi_2O_4$ catalyst, especially at lower conversion factors. However, this trend does not hold for all values of α. Interestingly, the reaction rate for the condition without catalyst is highest at α=0.75, while for the other two conditions, the highest reaction rate is observed at α=0.65. This suggests that the optimal conversion factor for the highest reaction rate may depend on the specific conditions and catalyst used.
Overall, this data provides valuable insights into the kinetics of sawdust under different conditions, which can be useful for optimizing the efficiency and effectiveness of sawdust conversion processes.

Figure 23.3 represents the results of the kinetic analysis of sawdust under three different conditions using the Friedman method.
The activation energy decreases as the conversion factor α increases for all three conditions. This suggests that the rate of decomposition of sawdust increases as the temperature increases. With $NiCa_2SiO_4$ catalyst, the activation energy is generally higher than with $NiCaOSi_2O_4$ catalyst, which in turn is generally higher than without catalyst. This suggests that the catalysts can lower the activation energy required for sawdust decomposition.
At α=0.9, the activation energy with $NiCa_2SiO_4$ catalyst is lower than without catalyst, while the activation energy with $NiCaOSi_2O_4$ catalyst is higher than with $NiCa_2SiO_4$ catalyst. This suggests that the effect of catalysts on activation energy may depend on the conversion factor α and the specific catalyst used.

Based on figure 22 data for sawdust with three different methods of kinetic analysis,
Flynn-Wall-Ozawa (FWO): This method calculates the activation energy by analyzing the conversion factor (α) as a function of temperature. In the provided data, the FWO method was applied to sawdust with and without catalysts, and two different catalysts were tested. The activation energies calculated using FWO ranged from approximately 79 to 221 kJ/mol for the three conditions, with the highest activation energy observed for sawdust without a catalyst at a conversion factor of 0.75. Overall, the FWO method appears to be useful for analyzing the effect of catalysts on the activation energy of the reaction.
Kissinger-Akahira-Sunose (KAS): This method uses the peak temperature of the derivative thermogravimetric (DTG) curve to calculate the activation energy. The provided data did not include KAS analysis for sawdust, so no comparison can be made for this method.
Friedman: This method involves plotting the logarithm of the heating rate against the reciprocal of the absolute temperature at the maximum rate of conversion to obtain a linear relationship, from which the activation energy can be calculated. The provided data for sawdust using the Friedman method showed activation energies ranging from approximately 52 to 284 kJ/mol for the three conditions, with the highest activation energy observed for sawdust with a

$NiCa_2SiO_4$ catalyst at a conversion factor of 0.9. Overall, the Friedman method appears to be useful for analyzing the overall activation energy of the reaction across different conditions.
In summary, each of these methods has its strengths and weaknesses, and the choice of method will depend on the specific research question and experimental setup. Based on the provided data, it appears that the FWO and Friedman methods are both useful for analyzing the activation energy of sawdust under different conditions.

Figure 24.1 represents the activation energy values for the conversion of cellulose using the KAS method for three different conditions: without catalyst, with $NiCaOSi_2O_4$ catalyst, and with $NiCa_2SiO_4$ catalyst.
For all three conditions, as the value of α (conversion factor) increases, the activation energy decreases, indicating that the reaction becomes more favourable at higher conversion rates.
The activation energy for cellulose conversion is lowest when using the $NiCaOSi_2O_4$ catalyst for all values of α. This suggests that $NiCaOSi_2O_4$ is the most effective catalyst among the three studied for promoting cellulose conversion. Without any catalyst, the activation energy is highest for all values of α, which suggests that the reaction rate is lowest without any catalyst present.
it can be concluded that the $NiCaOSi_2O_4$ catalyst is the most effective among the three studied catalysts for promoting cellulose conversion, especially at high conversion rates. However, if a moderate conversion rate is desired, the $NiCa_2SiO_4$ catalyst may be a better choice

Figure 24.2 represents the kinetics of cellulose decomposition under three different conditions using the FWO method of kinetic analysis. The three conditions are without catalyst, with $NiCaOSi_2O_4$ catalyst, and with $NiCa_2SiO_4$ catalyst. The conversion factor α is varied from 0.05 to 0.9.
From the data, it can be observed that the activation energy for cellulose decomposition decreases with the addition of catalysts for all values of α. This means that the catalysts facilitate the decomposition process and lower the energy barrier for cellulose decomposition.
The difference in the activation energy between the two catalysts is not significant, with $NiCaOSi_2O_4$ catalyst showing slightly better performance in some cases.
As the value of α increases, the activation energy for cellulose decomposition decreases, indicating that higher conversion rates require less energy to be supplied to the system.
Overall, the data shows that the addition of catalysts can improve the kinetics of cellulose decomposition, which could be useful in industrial processes that involve cellulose degradation

On the other hand, in the case of the Friedman (Figure24.3), it is observed that the catalyst $NiCaOSi_2O_4$ has a positive effect on the cellulose degradation, whereas the catalyst $NiCa_2SiO_4$ has a negative effect. This is evident from the fact that the activation energy required for cellulose degradation is lower in the presence of $NiCaOSi_2O_4$, but higher in the presence of $NiCa_2SiO_4$, as compared to the without catalyst condition. It is also observed that the reaction rate decreases as the conversion factor α increases, indicating that a higher conversion factor leads to a slower degradation of cellulose.

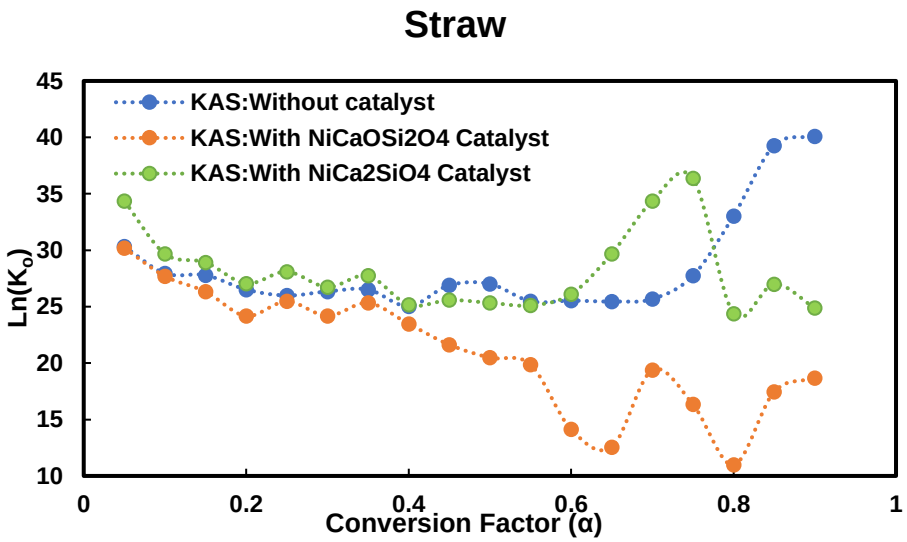

Figure 25.1
Change of Pre-exponential Factor of Straw with KAS method under three catalytic conditions

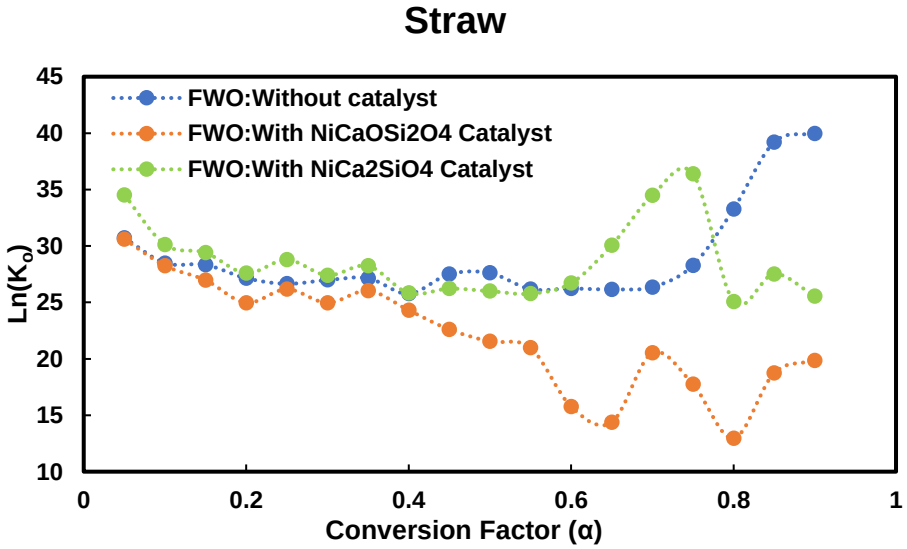

Figure 25.2
Change of Pre-exponential Factor of Straw with FWO method under three catalytic conditions

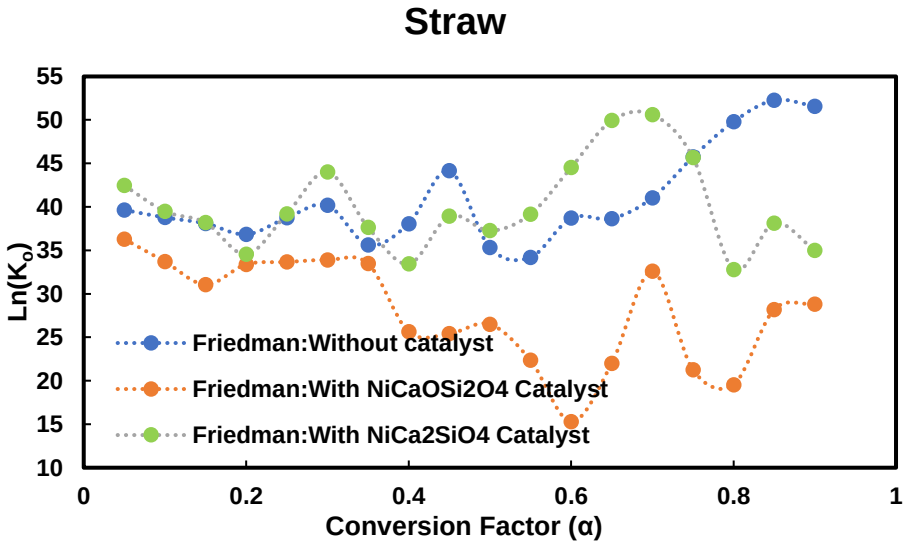

Figure 25.3
Change of Pre-exponential Factor of Straw with Friedman method under three catalytic conditions

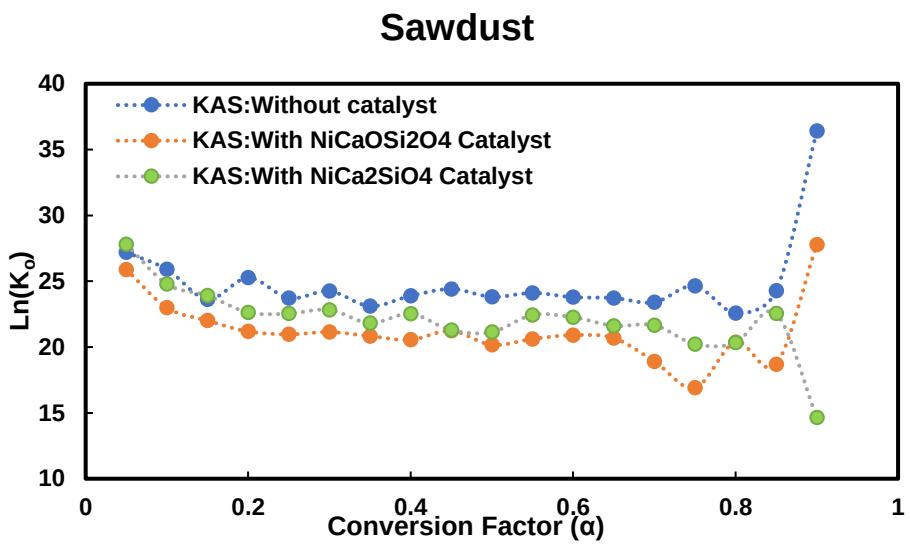

Figure 26.1
Change of Pre-exponential Factor of Sawdust with KAS method under three catalytic conditions

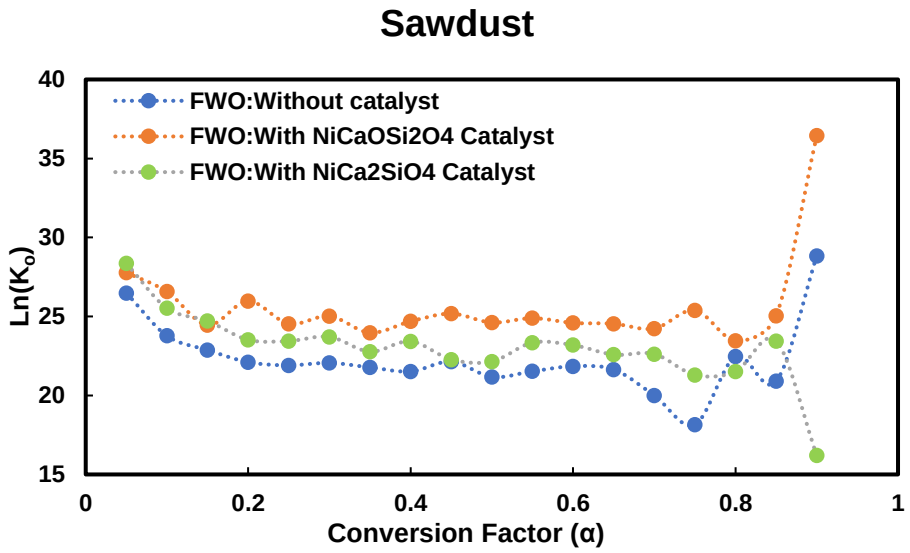

Figure 26.2
Change of Pre-exponential Factor of Sawdust with FWO method under three catalytic conditions

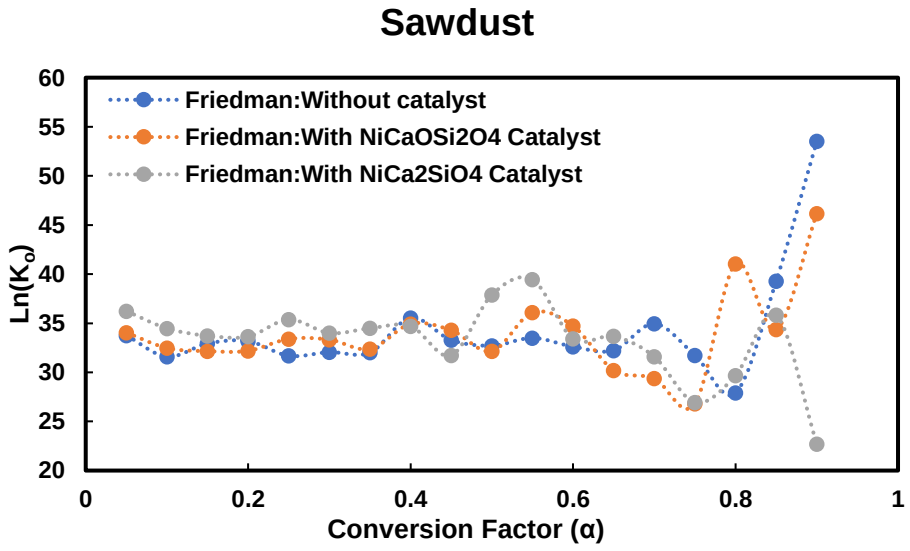

Figure 26.3
Change of Pre-exponential Factor of Sawdust with Friedman method under three catalytic conditions

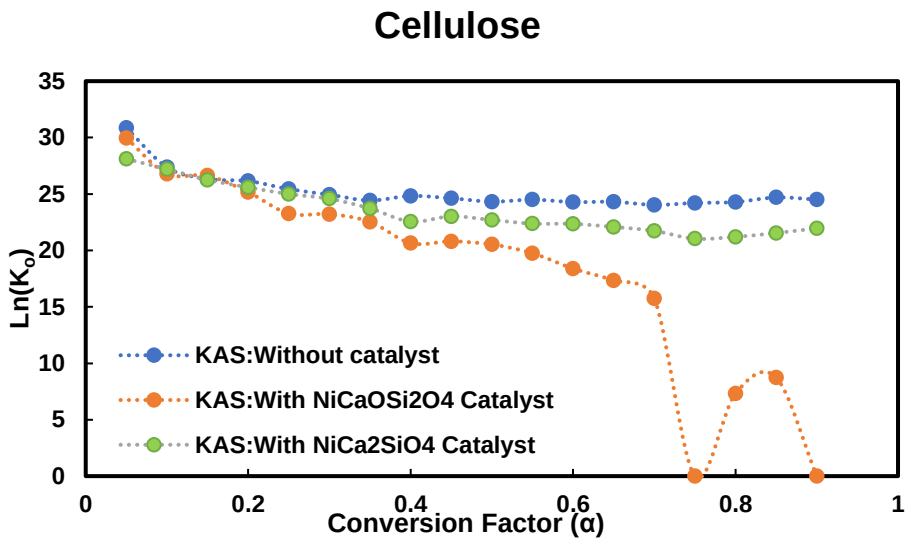

Figure 27.1
Change of Pre-exponetial factor of Cellulose with KAS method under three catalytic conditions

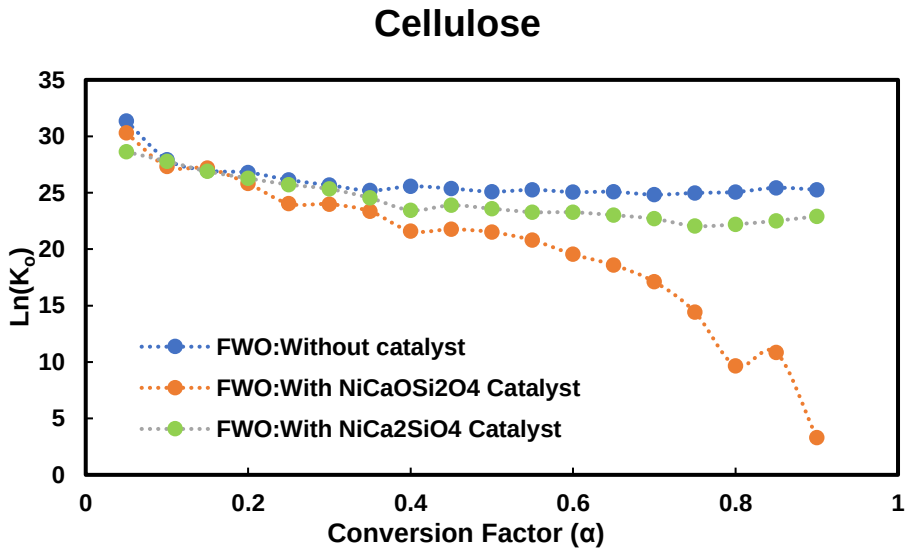

Figure 27.2
Change of Pre-exponential factor of Cellulose with FWO method under three catalytic conditions

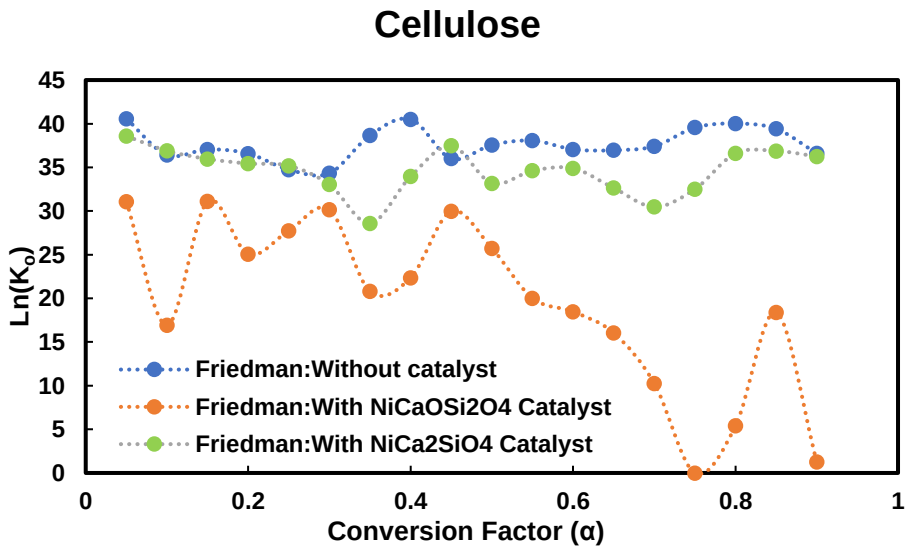

Figure 27.3
Change of pre-exponential factor of Cellulose with Friedman method under three catalytic conditions

Figure 25.1 represents the pre-exponential factor (K_o) for three different conditions of straw using the KAS method of kinetic analysis with a conversion factor (α).
The values of K_o are very high, ranging from 10^{11} to 10^{17}, indicating a very fast reaction rate. The values of K_o seem to decrease with increasing values of α for most of the conditions, indicating a decrease in the reaction rate with increasing conversion. There are some irregularities in the data, such as very high values for certain conditions, which could be due to experimental error or some other factors affecting the reaction rate.
Overall, the data suggests that the reaction rate for the straw under different conditions is very fast, but the reaction rate decreases with increasing conversion. However, further analysis and experiments would be needed to draw more definitive conclusions.

From Figure 25.2, we can see that there are three different conditions mentioned for the pre-exponential factor with respect to the conversion factor (α) using the Flynn-Wall-Ozawa (FWO) method. The conditions are Without catalyst, With $NiCaOSi_2O_4$ Catalyst, and With $NiCa_2SiO_4$ Catalyst.
Looking at the data, we can see that for each condition, as the conversion factor (α) increases, the pre-exponential factor decreases. This inverse relationship is expected as the activation energy increases with increasing α, leading to a slower reaction rate and a lower pre-exponential factor.
Furthermore, we can also observe that the pre-exponential factor values are different for each condition. This suggests that the presence of a catalyst can have a significant impact on the reaction rate and the pre-exponential factor.
In particular, we can see that the presence of $NiCa_2SiO_4$ catalyst leads to the lowest pre-exponential factor values, followed by $NiCaOSi_2O_4$ catalyst and without catalyst condition. This indicates that the $NiCa_2SiO_4$ catalyst is the most effective in enhancing the reaction rate and lowering the activation energy

Comparing the FWO and Friedman methods, it is observed that the values of K_o are generally higher for the Friedman method than the FWO method. This may be due to the fact that the Friedman method assumes a single reaction mechanism and does not consider the complexity of the reaction pathways. In contrast, the FWO method accounts for the multiple reaction pathways that may occur during the thermal degradation of straw.
The data also shows that the addition of catalysts ($NiCaOSi_2O_4$ and $NiCa_2SiO_4$) generally decreases the values of K_o, indicating that the presence of catalysts can slow down the rate of degradation. This may be due to the fact that the catalysts can inhibit the reaction by forming stable intermediates or by adsorbing the reactants and decreasing their availability.
Overall, the data provides insights into the thermal degradation of straw and the effect of catalysts on the reaction rate. The differences between the FWO and Friedman methods also highlight the importance of selecting an appropriate method for the kinetic analysis of complex reaction systems.

From the Figure 26.1, we can observe that the pre-exponential factor (K_o) for sawdust varies for different conditions (without catalyst, with $NiCaOSi_2O_4$ catalyst, and with $NiCa_2SiO_4$ catalyst) and different values of α (conversion factor) with the KAS method of kinetic analysis. We can see that the pre-exponential factor increases as the value of α increases for all three conditions. Also, we can observe that the pre-exponential factor is significantly higher for the $NiCa_2SiO_4$ catalyst condition as compared to the other two conditions for most of the values of α.
Furthermore, we can compare the pre-exponential factor for different conditions at a fixed value of α. For example, at α = 0.1, the pre-exponential factor for the $NiCa_2SiO_4$ catalyst

condition is significantly higher (5.79×10^{10}) than the other two conditions (9.59×10^{9} and 1.79×10^{11} for without catalyst and with $NiCaOSi_2O_4$ catalyst, respectively).
Overall, the KAS method of kinetic analysis shows how the pre-exponential factor varies with different conditions and values of α for sawdust. It also highlights that the choice of catalyst can significantly affect the pre-exponential factor.

Looking at the Figure 26.2 for pre-exponential factors for sawdust using the FWO method, we can observe the following insights:
The pre-exponential factors increase with increasing α conversion factor for all three conditions, i.e., without catalyst, with $NiCaOSi_2O_4$ catalyst, and with $NiCa_2SiO_4$ catalyst.
The pre-exponential factor values for the condition without
A catalyst are generally higher than the values for the conditions with the two different catalysts. This suggests that the catalysts may have a suppressing effect on the reaction rate. For the same value of α, the pre-exponential factor values for the condition with $NiCa_2SiO_4$ catalyst are generally higher than the values for the condition with $NiCaOSi_2O_4$ catalyst. This suggests that the $NiCa_2SiO_4$ catalyst may be more effective in promoting the reaction than the $NiCaOSi_2O_4$ catalyst. There are some notable fluctuations in the pre-exponential factor values with changing values of α. For example, for the condition without catalyst, the pre-exponential factor value for α=0.4 is significantly lower than the values for adjacent α values, which could indicate a change in the reaction mechanism or rate-limiting step at this particular α value.
Overall, these insights suggest that the FWO method can provide valuable information about the kinetic behaviour of the sawdust reaction, and that the choice of catalyst can have a significant impact on the reaction rate.

Figure 26.3 represents the pre-exponential factor (K_o) for the kinetic analysis of sawdust under three different conditions (without catalyst, with $NiCaOSi_2O_4$ catalyst, and with $NiCa_2SiO_4$ catalyst) using the Friedman method. The values of A for each condition are given for different values of conversion factor (α).

For the without catalyst condition, the values of K_o are generally higher at lower values of α and decrease as α increases. For the with $NiCaOSi_2O_4$ catalyst condition, the values of K_o increase steadily as α increases. For the with $NiCa_2SiO_4$ catalyst condition, the values of K_o show a more complex trend, with some fluctuations and peaks at certain values of α.
Overall, the data suggests that the presence of a catalyst can significantly enhance the reaction rate of sawdust, and the choice of catalyst can affect the optimal conditions for maximum reaction rate.

Looking at the Figure 27.1 for pre-exponential factor (K_o) for cellulose with three different catalyst conditions using the KAS method, we can make the following observations:
K_o decreases with increasing values of α in all three catalyst conditions. This trend is expected since the reaction rate decreases as the extent of reaction (α) increases. The pre-exponential factor (K_o) is significantly higher for cellulose without catalyst compared to the catalyst conditions. This indicates that the presence of a catalyst increases the reaction rate and reduces the activation energy required for the reaction. Among the two catalyst conditions, the $NiCaOSi_2O_4$ catalyst has a higher pre-exponential factor (K_o) compared to the $NiCa_2SiO_4$ catalyst for almost all values of α. This suggests that the $NiCaOSi_2O_4$ catalyst is more effective in promoting the reaction rate for cellulose. The values of pre-exponential factor (K_o) for cellulose with the $NiCa_2SiO_4$ catalyst exhibit some irregularities for higher values of α, which may indicate some limitations of the KAS method for this particular catalyst condition.

Overall, the data suggests that the presence of a catalyst can significantly enhance the reaction rate for cellulose and that the choice of catalyst can have a significant impact on the pre-exponential factor. The KAS method can provide useful insights into the kinetics of the reaction, but some caution should be exercised in interpreting the data, especially for catalyst conditions where the data may exhibit some irregularities.

Figure 27.2 represents the pre-exponential factor (K_o) for cellulose decomposition under three different conditions using the FWO (Flynn-Wall-Ozawa) method of kinetic analysis. Here are some insights from the data:
The pre-exponential factor (K_o) is higher for cellulose decomposition without any catalyst than with either $NiCaOSi_2O_4$ or $NiCa_2SiO_4$ catalysts. This suggests that the presence of these catalysts may not enhance the cellulose decomposition rate significantly. K_o decreases with an increase in the temperature, which is expected since the reaction rate usually increases with an increase in temperature due to the activation energy. The K_o values for cellulose decomposition with $NiCaOSi_2O_4$ catalyst are slightly higher than with $NiCa_2SiO_4$ catalyst for most of the conversion factors. This may indicate that $NiCaOSi_2O_4$ catalyst is more effective in promoting cellulose decomposition than $NiCa_2SiO_4$ catalyst.
Overall, the FWO method provides valuable information on the kinetics of cellulose decomposition under different conditions, which can be useful in optimizing the reaction conditions for industrial applications.

Figure 27.3 shows the pre-exponential factor for cellulose under three different conditions with the Friedman method of kinetic analysis.
For the condition without catalyst, the pre-exponential factor is the highest at every α value, indicating that the reaction rate is highest without any catalyst present. For the condition with $NiCa_2SiO_4$ catalyst, the pre-exponential factor is the lowest at every α value, indicating that the reaction rate is lowest with this particular catalyst. The effect of the $NiCaOSi_2O_4$ catalyst on the pre-exponential factor is mixed, with some values being higher and others being lower than the condition without catalyst.

It's important to note that the pre-exponential factor is only one part of the Arrhenius equation and does not give a complete picture of the reaction rate. Other factors such as activation energy and temperature must also be taken into account.

4.11.Discussions:

Four model-free iso-conversion approaches were used to analyse the kinetics of biomass catalytic pyrolysis at various conversion(α) levels, from 0.05 to 0.90. above figure shows results obtained for all biomasses under different catalytic conditions were transformed into Arrhenius plot for cellulose, sawdust, and straw with three conditions that is (1) no catalyst (2) Ni-CaO-Ca_2SiO_4, (3) Ni-Ca_2SiO_4 with Five methods DAEM, KAS, FWO, Friedman & Starink where the arrow means the increasing direction of conversion α in an interval of 0.05. calculated activation energy E, Pre-exponential Factor and correlation R^2 of all samples with Four methods is listed in Table 4-12. And overall correlation was above 0.9 which indicates that all Four methods are suitable for modelling catalytic biomass pyrolysis. Above tables indicates that cellulose under three cases was easier to model by DAEM methods as compared to sawdust and straw due to higher correlation (R^2), which may due to complex organic composition. It was evident from the activation energy measured under various catalytic circumstances that the functional materials Ni-CaO-Ca_2SiO_4 and Ni-Ca_2SiO_4 both reduced the activation energy of pyrolysis. The range of E for the pyrolysis of cellulose using Ni-Ca_2SiO_4 was between 100 and 158 kJ/mol. At conversion α = 0.05-0.9 decrease in E indicates that catalytic effect of Ni on O-H and C-H. Activation Energy E of sawdust without catalyst was found to increase with conversion over the conversion range of 0.10 to 0.85, while the lowest E was 131.1 kJ/mol (DAEM) and the highest is 148.1 kJ/mol. Both Ni-CaO-Ca_2SiO_4 and Ni-Ca_2SiO_4 had similar impacts on activation energy during the conversion range α = 0.05-0.65. Over the conversion range α = 0.65-0.85, sawdust with Ni-CaO-Ca_2SiO_4 had a lower activation energy than sawdust with Ni-Ca_2SiO_4, which might be explained by the presence of CaO, which can encourage the cracking of small organic molecules from the pyrolysis of big organic molecules.

In this above discussion we studied three kinds of biomasses i.e. (cellulose, sawdust and straw) in three catalytic condition that is no catalyst, Ni-CaO-Ca_2SiO_4, Ni-Ca_2SiO_4 were investigated by TGA. For three types tested, functional material CaO-Ca_2SiO_4 showed greatest catalytic effect on pyrolysis due to decrease in activation energy. For cellulose and sawdust functional material Ni-Ca_2SiO_4 also showed variation of measured activation energy. For straw
Ni-Ca_2SiO_4 resulted in increase in activation energy, may be because of higher inorganic content of straw The correlation R^2 of all fitting lines was greater than 0.9 in all cases, indicating that the DAEM were appropriate for predicting the kinetics of biomass catalytic pyrolysis. With conversion and the inclusion of functional ingredients, the activation energy curves exhibited a continuous trend. The pre-exponential factor is an important kinetic parameter in the modeling of chemical reactions. In this case, we are comparing the results of three different methods for determining the pre-exponential factor for cellulose: KAS, FWO, and Friedman. Looking at the data Calculated, we can see that the values of the pre-exponential factor obtained using the three methods are quite different, especially for the higher values of α. For example, at α=0.8, Sawdust with Ni-CaOSi_2O_4 Catalyst condition, the pre-exponential factor obtained using KAS is $7.04x10^{14}$, while the values obtained using FWO and Friedman are $1.54x10^{10}$ and $6.66\ x10^{17}$, respectively.
These differences can be attributed to the assumptions and approximations made by each method. For instance, the KAS method assumes that the reaction is a single-step process with constant activation energy, whereas the FWO method takes into account the possibility of multiple steps with varying activation energies.

Similarly, the Friedman method assumes that the reaction follows an nth-order kinetic model with respect to the reactant concentration, whereas the other two methods do not make any assumptions about the reaction order.

Therefore, it is important to carefully choose the appropriate method based on the reaction mechanism and experimental conditions. Additionally, it is recommended to use multiple methods to cross-check the results and ensure the reliability of the obtained values. Overall, the comparison of the three methods shows that there can be significant variations in the obtained pre-exponential factors, highlighting the importance of choosing an appropriate method and conducting a thorough analysis of the experimental data.

Based on Master plot, it appears that the use of different catalysts can significantly alter the reaction mechanism of pyrolysis in the conversion of biomass into biofuels. The master plots obtained from the experiments revealed that for each type of biomass, with or without a catalyst, different reaction mechanisms were observed at different stages of the conversion process.

For instance, when pyrolyzing straw biomass, $NiCaOSi_2O_4$ catalyst altered the reaction mechanism such that it was majorly governed by 5^{th} order (R5) and third-order (R3) with nucleation reaction and diffusion-controlled mechanisms. In contrast, pyrolyzing straw without catalyst showed the diffusion-controlled random nucleation mechanism and was majorly governed by second order (R2) reactions. Similarly, for sawdust biomass, the addition of $NiCaOSi_2O_4$ catalyst led to 4^{th} order (R4) chemical reaction with diffusion-controlled nucleation mechanism, while the absence of a catalyst followed a one and a half order reaction (R6) with diffusion-controlled mechanism. In the case of Cellulose without Catalyst, the overall process followed Avarami-erofeev sigmoidal rate equation with random nucleation mechanism and diffusion-controlled mechanism. However, in the presence of $NiCaOSi_2O_4$ Catalyst, the process followed Avarami-erofeev sigmoidal rate equation and random nucleation mechanism in overall conversion, and a 3rd order reaction mechanism with random nucleation for the final stage. This indicates that the use of $NiCaOSi_2O_4$ Catalyst altered the reaction mechanism, making it more favorable for producing targeted biofuels.

Similarly, in the presence of $NiCa_2SiO_4$ Catalyst, the process followed Avarami-erofeev sigmoidal rate equation till 65% conversion, and then showed a random nucleation mechanism at 50% conversion, diffusion-controlled mechanism at 75% to 80% conversion, and Prout-Tomkins random nucleation mechanism at the final conversion. The prediction made by the master plot shows strong control of the Avarami-erofeev sigmoidal rate equation, indicating the importance of the plot in understanding the reaction mechanism.

In summary, the use of different catalysts alters the reaction mechanisms governing the pyrolysis of biomass, and the choice of catalyst could significantly affect the yield and quality of the targeted biofuels.

Conclusion:

The pyrolysis behaviours of three types of biomasses (cellulose, sawdust, and straw) have been studied using the model free isoconversional technique under three catalytic conditions (no catalyst, Ni-$CaOCa_2SiO_4$, and Ni-Ca_2SiO_4) and reaction mechanism by Master plot.

- The functional materials, Ni-$CaOCa_2SiO_4$ and Ni-Ca_2SiO_4, showed an obvious catalytic effect for the three types of biomass samples tested.
- The correlation R^2 of all fitting lines in all cases was above 0.9, which indicated that FWO method, KAS method, Friedman method and DAEM were suitable for modelling the kinetics of biomass catalytic pyrolysis whereas FWO method, KAS method, DAEM showed more accuracy as compare Friedman method.
- For the three types of biomasses tested, the functional material, $NiCaOCa_2SiO_4$, showed the greatest catalytic effect on pyrolysis due to the evident decrease in activation energy. For sawdust, the functional material, Ni-Ca_2SiO_4 Catalyst showed Greater catalytic effect as compared to , $NiCaOCa_2SiO_4$ Catalyst.
- significant impact of catalysts on the reaction mechanisms. The use of $NiCaOSi_2O_4$ catalyst altered the reaction pathway, with involvement of nucleation, diffusion control, and multiple reaction mechanisms. The presence of catalysts provided better control over the conversion process and facilitated the production of targeted biofuels.

References:

[1] :Liu, C., Wang, H., Karim, A. M., Sun, J., & Wang, Y. (2014). Catalytic fast pyrolysis of lignocellulosic biomass. Chemical Society Reviews, 43(22), 7594-7623.

[2]: H.B. Mayes, L.J. Broadbelt, Unraveling the reactions that unravel cellulose, J. Phys. Chem. 116 (2012) 7098–7106, https://doi.org/10.1021/jp300405x.

[3]: Yang, Hang, et al. "Kinetics of catalytic biomass pyrolysis using Ni-based functional materials." Fuel Processing Technology 195 (2019): 106145.

[4]: H.E. Kissinger, Reaction kinetics in differential thermal analysis, Anal. Chem. 29 (1957) 1702–1706.

[5]: J.H. Flynn, L.A. Wall, General treatment of the thermogravimetry of polymers, Journal of Research of the National Bureau of Standards Section A: Physics and Chemistry 70A (1966) 487–523.

[6]: M.J. Starink, A new method for the derivation of activation energies from experiments performed at constant heating rate, Thermochim. Acta 288 (1996) 97–104

[7]: K. Miura, T. Maki, A simple method for estimating f(E) and k0(E) in the distributed activation energy model, Energy Fuel 12 (1998) 864–869

[8]: 13 H. L. Friedman, J. Polym. Sci., 6C (1965) 183.

[9]: F. Gotor, J. Criado, J. Malek Kinetic analysis of solid-state reactions: the universality of master plots for analyzing isothermal and nonisothermal experiments J. Phys., 104 (2000), pp. 10777-10782

[10]: Khawam, A., Flanagan, D.R., 2006. Solid-state kinetic models: Basics and mathematical fundamentals. J. Phys. Chem. B 110 (35), 17315–17328